Based on the comparison between SDM and the HLA-DR1/SEB complex, the binding of SDM to the α-chain of MHCII is unlikely. MHCII α-chain-binding regions of SEB and analogous areas of SDM present significant differences. SDM residues Ile29, Gly30, and Thr31 are less hydrophobic than, and positioned differently from, the structurally equivalent residues Phe44, Leu45, and Phe47 of SEB. Glu67 of SEB is replaced by Asn56 in SDM, a change that disables the ability of SDM to form a salt bridge with Lys39 of the MHC α-chain. The region corresponding to the disulphide loop of SEB between residues 93 and 115 is completely different from the SDM structure. Major differences in all sites involved in HLA-DR1 binding can be seen, and this provides further support for an MHCII binding mode in SDM different from that in SEB. Additional evidence for the MHCII β-chain binding of SDM was gained from mutagenesis experiments where the mutation of His170 to alanine resulted in a reduced mitogenic activity (Fig. 5).

Based on the similarity of the zinc-binding site with that of other superantigens that bind through the MHCII β-chain, a zinc-dependent SDM binding to MHCII and similar MHCII β-chain-binding properties for SDM can be suggested. In addition to His81 of the MHCII β-chain as a zinc ligand, other residues at the interface may be able to form bonds with the MHCII β-chain. The superantigen residues involved in hydrogen-bond formation with the β-chain are Asn105, Lys163, Asp164, Ser200, and Asp203 of SPE-C when SPE-C is cocrystallized with HLA-DR2a and MBP antigen peptide,[28] and Asn113, Arg127, and Ser205 of SEH in the SEH/HA/HLA-DR-1 complex.[29] Structural comparisons with other superantigens that bind to MHCII in a zinc-dependent manner showed that an asparagine equivalent to SDM Asn111 is conserved in all those superantigens. A hydrogen bond between the MHCII β-chain and the side chain of this asparagine can be formed as described by modelling. Thus, Asn111 could have some significance in SDM binding to the MHCII molecule.

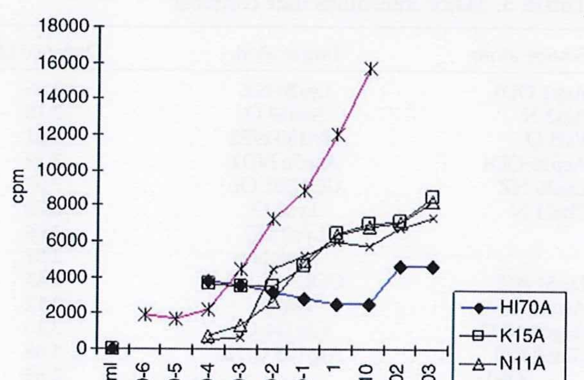

Fig. 5. T-cell-stimulating activity of wild-type and mutant SDM. Human peripheral blood mononuclear cells (1×10^5 cells/well in 96-well plates) were stimulated with various doses of SDM for 3 days and examined for mitogenic response as described in Experimental Procedures.

Other superantigen residues forming hydrogen bonds in SPE-C/MBP/HLA-DR2a and SEH/HA/HLA-DR1 complexes are less conserved, and the course of the main chains can vary slightly. This indicates that residues involved in hydrogen-bond formation can be different, the number of hydrogen bonds could vary, and the angle of binding may not be the same. Each of the SPE-C residues involved in zinc-dependent MHCII binding has the same residue in the structurally equivalent position in SDM (Asn111, Lys172, Asp173, Ser199, and Asp202), with the orientations of these residues being similar in both SDM and SPE-C. The comparison of the SEH/HA/HLA-DR1 complex and SDM showed that the residue analogous to the hydrogen-bonding Arg127 of SEH is Thr128 in SDM. Structural comparisons also suggest that the binding angle of SDM may be different or that residues not involved in hydrogen-bond formation in other superantigens can instead take part in SDM–MHCII interactions. Details of the binding mode of SDM are still unknown, and further examination is certainly required.

Structural studies of superantigen/MHCII complexes have shown that superantigens also interact with the peptide antigen (e.g., MBP peptide, HA peptide, or a collagen II peptide) bound to the MHCII molecule.[4,30] Gln120 of SEH—as well as Gln113 of SPE-C, which is aligned with Gln120 of SEH at the structural but not at the sequence level—has been shown to be an important residue for peptide binding.[8] A glutamine residue analogous to SEH Gln120 is conserved in most superantigens that bind to the MHCII β-chain but is absent in SPE-G, SPE-L, SPE-M, and SDM. SPE-C Gln113 forms two hydrogen bonds with MBP peptide antigen backbone atoms in the HLA-DR2a/MBP/SPE-C complex. A model of SDM/MBP/HLA-DR2a based on the SPE-C/MBP/HLA-DR2a complex structure reveals significant differences at the interface between these two structures, most importantly the absence of an SDM residue that is structurally equivalent to SPE-C Gln113. Compared to SEH, the side chain of SDM Gln122 is located in the same area as the SEH Gln120 side chain, but it is almost perpendicular to it after structural superposition. However, this does not exclude the possibility that SDM Gln122 could act as SEH Gln120 and SPE-C Gln113, thus enabling a similar binding mode, although the binding angle of the peptide would probably be different. Moreover, it is still possible that SDM may interact with an antigen peptide in a different way or may be unable to form bonds with particular peptides. Nevertheless, the general strategy adopted by superantigens that bind to the MHCII β-chain to minimise specific interactions with the side chains of the peptide antigen[30] appears highly likely for SDM as well.

TcR binding

SDM binds specifically to human Vβ1.1- and Vβ23-chains, a repertoire shared only by a few superantigens. No superantigen/TcR complex structure containing one of those Vβ-chains has yet been determined. Thus, structural comparisons and modelling cannot give precise predictions. However, and in order to gain structural insights, SDM was superimposed onto SPE-C and SPE-A from the SPE-C/TcR hVβ2.1 and SPE-A/TcR mVβ8.2 complexes, respectively.[11] Based on these comparisons, residues of SDM were identified and mutagenesis experiments were performed to obtain information on their role in the mitogenic activity of SDM.

SPE-C Tyr15, SPE-J Tyr14, SPE-A Asn20, and SEB/SEC2/SEC3 Asn23 have been previously shown to be involved in TcR binding. Moreover, mutations of SEC3 Asn23Ala and SPE-J Tyr14Ala result in a significant decrease in the mitogenic capacity of these superantigens.[31,32] All residues mentioned above are structurally conserved. Furthermore, SDM Asn11 shares the same location with the above residues. The mutation of Asn11 to Ala, however, resulted in a protein with similar mitogenic activity as the wild type (Fig. 5).

Another important residue for TcR binding is located in the α5 helix and corresponds to either glutamine (SPE-A Gln194 and SEB/SEC2/SEC3 Gln210) or arginine (SPE-C/SPE-J Arg181). Mutants (Gln210Ala of SEC3 and Arg181Gln of SPE-J) showed an almost complete loss of mitogenic capacity. The lack of the α5 helix in SDM raises the question of whether SDM has a different TcR binding mode compared to many other superantigens. The side chain of SDM Lys15 is located in the same area, with the hydrogen bond forming residues from the α5 helix; thus, Lys15 of SDM could participate in hydrogen-bond formation with TcR. The mutation of Lys15 to Ala caused no decrease in the mitogenic capacity (Fig. 5), suggesting that this residue is not crucial for TcR interactions. TSST-1 is also characterized by the lack of a similar helix in its structure. However, there are no currently available data suggesting SDM binding to TcR similar to that found for TSST-1.[33] Structural superposition of SDM onto TSST-1 (sequence identity = 19.7%; RMSD = 2.02 Å) of the TSST-1/D10 hVβ2.1 complex shows large deviations (up to 7 Å) in loops contacting D10; thus, no reliable predictions can be drawn.

A ternary complex of MHCII molecule, superantigen, and TcR can be formed in several ways, depending on the superantigen. SPE-C acts as a bridge between MHC and TcR, and these molecules cannot have any direct contacts between them. SEB instead allows contacts between the TcR Vα-chain and the MHC β-chain. The unknown location of TcR binding on SDM makes it impossible to predict the exact geometry of the ternary complex that SDM could form.

Conclusions

SDM shares the characteristic superantigen fold, except that it lacks the α5 helix present in other superantigens. In addition, SDM exhibits a zinc-binding site as identified by the presence of a bound zinc ion in the structure. Based on structural comparisons, binding to MHCII molecules is mediated in a zinc-dependent manner involving the β-chain of the MHCII molecule. The binding most likely takes place in a similar way as in SPE-C and SEH, although the binding angle is probably different and the peptide affects the SDM-binding properties. The TcR Vβ-chain binding mode is less easily predicted, and mutagenesis experiments suggest that SDM does not share the same TcR-binding properties with many other superantigens.

Experimental Procedures

Purification and crystallization

Recombinant SDM was expressed, purified, and crystallized as previously described.[34] Briefly, the protein was concentrated to 10 mg/ml prior to crystallization in Na-acetate buffer (pH 5). Crystals were grown with the hanging-drop vapour diffusion method at 16 °C using a reservoir solution containing 18–20% polyethylene glycol 3350 and 0.4 M lithium nitrate (pH 4.2–4.6). Crystals appeared after ~5 days.

X-ray data collection

A complete data set to 1.9 Å resolution was collected on beamline X11 at the European Molecular Biology Laboratory (EMBL) Hamburg (care of Deutsches Elektronen Synchrotron). Prior to data collection, a single SDM crystal was flash-cooled to 100 K using 20% glycerol as cryoprotectant. Diffraction data were recorded on a 165-mm MarCCD detector using a Δφ of 0.5°, a crystal-to-detector distance of 175 mm, and a wavelength of 0.8123 Å. The data were integrated, merged, and scaled using the HKL program suite.[35] The TRUNCATE program from the CCP4 program suite[36] was used to convert intensities to amplitudes. Anomalous data on the zinc peak edge (λ = 1.2824 Å) were collected at station BW7A (EMBL Hamburg). A total of 1700 images were collected (0.5° rotation per image). Calculation of the anomalous difference electron density map was carried out with programs from the CCP4i.[36]

Structure determination, refinement, and quality of the models

Initial phases were obtained using molecular replacement. The program PHASER[37] was employed, and a polyalanine model of SPE-C without water molecules, zinc, and highly flexible surface loops was used in the search. To resolve the ambiguity in the space group, the search was carried out in $P3$, $P3_1$, and $P3_2$ space groups. The best solution was obtained in space group $P3_2$. The structure was refined using CNS v. 1.1.[38] A subset

(5%) of the total number of reflections was randomly selected and set aside for cross-validation analysis to monitor the progress of refinement using the R_{free} factor.[39] Initial rebuilding and refinement were carried out using data to 2.4 Å resolution. When a new data set to 1.9 Å resolution was collected, the resolution was extended in steps of 0.1 Å. Reflections from 1.95 to 1.90 Å were not used due to high R_{sym} and low I/σ ratio.

The models were visualized with the program O.[40] Working and reference sets were merged only in the final refinement run. The quality of the model was checked using PROCHECK.[21] The RMSDs from ideal geometry and Luzzati plots were calculated using CNS. LSQMAN[41] was used for structural superposition and calculation of RMSD for particular loops. Crystal contacts were determined with the program CONTACT.[36] Secondary structure elements were analyzed with DSSP.[42] Structure-based alignment was performed using the protein structure comparison server SSM[43] at the European Bioinformatics Institute‡ and was inspected on graphics.

Preparation of SDM mutants containing single-amino-acid substitution

To introduce single-amino-acid substitution into the SDM molecule, PCR-based mutagenesis was performed. All amplified fragments were digested with restriction enzymes as described by the restriction sites introduced into the PCR primers and subcloned into TAGZyme pGE2 (QIAGEN) to construct expression plasmids. In the case of the *H170A* mutant, the N- and C-terminals of SDM were amplified separately and digested with restriction enzymes. The resulting plasmids were used for the transformation of TOP10 cells (Invitrogen). After the verification of the plasmid carrying each mutation by sequencing using BigDye v. 3.1 and 3100 Genetic analyzer (Applied Biosystems), the mutant SDM proteins were expressed and purified as previously reported.[34]

Mitogenic activity assay of SDM

To assay the mitogenic activity of SDM, human peripheral blood mononuclear cells (1×10^5 cells) were stimulated in triplicate with mitogens in 0.2-ml volumes in 96-well round-bottom microplates for 3 days. The cultures were pulsed with [^{3}H] thymidine for the last 16 h of cultivation, and incorporation of radioactivity was measured as previously described.[44]

Data deposition

Atomic coordinates and structure factors have been deposited with the Rutgers Protein Data Bank under accession code 2J4X.

‡ http://www.ebi.ac.uc/msd-srv/ssm

Acknowledgements

This work was supported by the Sigrid Jusélius Foundation. We thank the staff at the Department of Analytical Chemistry at Åbo Akademi for assistance with direct coupled plasma measurements and the staff at EMBL Hamburg for help with data collection. Access to EMBL Hamburg/Deutsches Elektronen Synchrotron (European Community—Access to Research Infrastructure Action of the Improving Human Potential Program to the EMBL Hamburg Outstation, contract no. HPRI-CT-1999-00017) is greatly acknowledged.

References

1. Proft, T. & Fraser, J. D. (2003). Bacterial superantigens. *Clin. Exp. Immunol.* **133**, 299–306.
2. Papageorgiou, A. C. & Acharya, K. R. (2000). Microbial superantigens: from structure to function. *Trends Microbiol.* **8**, 369–375.
3. Proft, T. & Fraser, J. D. (2007). Streptococcal superantigens. *Chem. Immunol. Allergy*, **93**, 1–23.
4. Petersson, K., Forsberg, G. & Walse, B. (2004). Interplay between superantigens and immunoreceptors. *Scand. J. Immunol.* **59**, 345–355.
5. Torres, B. A., Kominsky, S., Perrin, G. Q., Hobeika, A. C. & Johnson, H. M. (2001). Superantigens: the good, the bad, and the ugly. *Exp. Biol. Med. (Maywood)*, **226**, 164–176.
6. Jardetzky, T. S., Brown, J. H., Gorga, J. C., Stern, L. J., Urban, R. G., Chi, Y. I. *et al.* (1994). Three-dimensional structure of a human class II histocompatibility molecule complexed with superantigen. *Nature*, **368**, 711–718.
7. Li, Y., Li, H., Dimasi, N., McCormick, J. K., Martin, R., Schuck, P. *et al.* (2001). Crystal structure of a superantigen bound to the high-affinity, zinc-dependent site on MHC class II. *Immunity*, **14**, 93–104.
8. Petersson, K., Hakansson, M., Nilsson, H., Forsberg, G., Svensson, L. A., Liljas, A. & Walse, B. (2001). Crystal structure of a superantigen bound to MHC class II displays zinc and peptide dependence. *EMBO J.* **20**, 3306–3312.
9. Zhao, Y., Li, Z., Drozd, S. J., Guo, Y., Mourad, W. & Li, H. (2004). Crystal structure of *Mycoplasma arthritidis* mitogen complexed with HLA-DR1 reveals a novel superantigen fold and a dimerized superantigen–MHC complex. *Structure*, **12**, 277–288.
10. Fields, B. A., Malchiodi, E. L., Li, H., Ysern, X., Stauffacher, C. V., Schlievert, P. M. *et al.* (1996). Crystal structure of a T-cell receptor beta-chain complexed with a superantigen. *Nature*, **384**, 188–192.
11. Sundberg, E. J., Li, H., Llera, A. S., McCormick, J. K., Tormo, J., Schlievert, P. M. *et al.* (2002). Structures of two streptococcal superantigens bound to TcR beta chains reveal diversity in the architecture of T cell signaling complexes. *Structure*, **10**, 687–699.
12. Li, H., Llera, A., Tsuchiya, D., Leder, L., Ysern, X., Schlievert, P. *et al.* (1998). Three-dimensional structure of the complex between a T cell receptor beta chain and the superantigen staphylococcal enterotoxin B. *Immunity*, **9**, 807–816.
13. Abrahmsén, L., Dohlsten, M., Segrén, S., Björk, P., Jonsson, E. & Kalland, T. (1995). Characterization of two distinct MHC class II binding sites in the

superantigen staphylococcal enterotoxin A. *EMBO J.* **14**, 2978–2986.
14. Herman, A., Labrecque, N., Thibodeau, J., Marrack, P., Kappler, J. W. & Sekaly, R. P. (1991). Identification of the staphylococcal enterotoxin A superantigen binding site in the beta 1 domain of the human histocompatibility antigen HLA-DR. *Proc. Natl. Acad. Sci. USA*, **88**, 9954–9958.
15. Fraser, J. D., Urban, R. G., Strominger, J. L. & Robinson, H. (1992). Zinc regulates the function of two superantigens. *Proc. Natl. Acad. Sci. USA*, **89**, 5507–5511.
16. Karp, D. R. & Long, E. O. (1992). Identification of HLA-DR1 beta chain residues critical for binding staphylococcal enterotoxins A and E. *J. Exp. Med.* **175**, 415–424.
17. Igwe, E. I., Shewmaker, P. L., Facklam, R. R., Farley, M. M., van Beneden, C. & Beall, B. (2003). Identification of superantigen genes *speM*, *ssa*, and *smeZ* in invasive strains of beta-hemolytic group C and G streptococci recovered from humans. *FEMS Microbiol. Lett.* **229**, 259–264.
18. Miyoshi-Akiyama, T., Zhao, J., Kato, H., Kikuchi, K., Totsuka, K., Kataoka, Y. *et al.* (2003). *Streptococcus dysgalactiae*-derived mitogen (SDM), a novel bacterial superantigen: characterization of its biological activity and predicted tertiary structure. *Mol. Microbiol.* **47**, 1589–1599.
19. McCormick, J. K., Yarwood, J. M. & Schlievert, P. M. (2001). Toxic shock syndrome and bacterial superantigens: an update. *Annu. Rev. Microbiol.* **55**, 77–104.
20. Brouillard, J. N., Gunther, S., Varma, A. K., Gryski, I., Herfst, C. A., Rahman, A. K. *et al.* (2007). Crystal structure of the streptococcal superantigen SpeI and functional role of a novel loop domain in T cell activation by group V superantigens. *J. Mol. Biol.* **367**, 925–934.
21. Laskowski, R. A., MacArthur, M. W., Moss, D. S. & Thornton, J. M. (1993). PROCHECK: a program to check the stereochemical quality of protein structures. *J. Appl. Crystallogr.* **26**, 283–291.
22. Baker, M. D., Gendlina, I., Collins, C. M. & Acharya, K. R. (2004). Crystal structure of a dimeric form of streptococcal pyrogenic exotoxin A (SpeA1). *Protein Sci.* **13**, 2285–2290.
23. Proft, T., Webb, P. D., Handley, V. & Fraser, J. D. (2003). Two novel superantigens found in both group A and group C *Streptococcus*. *Infect. Immun.* **71**, 1361–1369.
24. Arcus, V. L., Proft, T., Sigrell, J. A., Baker, H. M., Fraser, J. D. & Baker, E. N. (2000). Conservation and variation in superantigen structure and activity highlighted by the three-dimensional structures of two new superantigens from *Streptococcus pyogenes*. *J. Mol. Biol.* **299**, 157–168.
25. Roussel, A., Anderson, B. F., Baker, H. M., Fraser, J. D. & Baker, E. N. (1997). Crystal structure of the streptococcal superantigen SPE-C: dimerization and zinc binding suggest a novel mode of interaction with MHC class II molecules. *Nat. Struct. Biol.* **4**, 635–643.
26. Kumaran, D., Eswaramoorthy, S., Furey, W., Sax, M. & Swaminathan, S. (2001). Structure of staphylococcal enterotoxin C2 at various pH levels. *Acta Crystallogr. Sect. D: Biol. Crystallogr.* **57**, 1270–1275.
27. Harding, M. M. (2001). Geometry of metal–ligand interactions in proteins. *Acta Crystallogr. Sect. D: Biol. Crystallogr.* **57**, 401–411.
28. Li, Y., Li, H., Dimasi, N., McCormick, J., Martin, R., Schuck, P. *et al.* (2001). Crystal structure of a superantigen bound to the high-affinity, zinc-dependent site on MHC class II. *Immunity*, **14**, 93–104.
29. Petersson, K., Håkansson, M., Nilsson, H., Forsberg, G., Svensson, L., Liljas, A. & Walse, B. (2001). Crystal structure of a superantigen bound to MHC class II displays zinc and peptide dependence. *EMBO J.* **20**, 3306–3312.
30. Fernández, M., Guan, R., Swaminathan, C., Malchiodi, E. & Mariuzza, R. (2006). Crystal structure of staphylococcal enterotoxin I (SEI) in complex with a human major histocompatibility complex class II molecule. *J. Biol. Chem.* **281**, 25356–25364.
31. Leder, L., Llera, A., Lavoie, P. M., Lebedeva, M. I., Li, H., Sekaly, R. P. *et al.* (1998). A mutational analysis of the binding of staphylococcal enterotoxins B and C3 to the T cell receptor beta chain and major histocompatibility complex class II. *J. Exp. Med.* **187**, 823–833.
32. Baker, H. M., Proft, T., Webb, P. D., Arcus, V. L., Fraser, J. D. & Baker, E. N. (2004). Crystallographic and mutational data show that the streptococcal pyrogenic exotoxin J can use a common binding surface for T-cell receptor binding and dimerization. *J. Biol. Chem.* **279**, 38571–38576.
33. Moza, B., Varma, A. K., Buonpane, R. A., Zhu, P., Herfst, C. A., Nicholson, M. J. *et al.* (2007). Structural basis of T-cell specificity and activation by the bacterial superantigen TSST-1. *EMBO J.* **26**, 1187–1197.
34. Papageorgiou, A. C., Saarinen, S., Ramirez-Bartutis, R., Kato, H., Uchiyama, T., Kirikae, T. & Miyoshi-Akiyama, T. (2006). Expression, purification and crystallization of *Streptococcus dysgalactiae*-derived mitogen. *Acta Crystallogr. Sect. F: Struct. Biol. Cryst. Commun.* **62**, 242–244.
35. Otwinowski, Z. & Minor, W. (1997). Processing of X-ray diffraction data collected in oscillation mode. *Methods in Enzymology*, vol. 276, pp. 307–326.
36. Potterton, E., Briggs, P., Turkenburg, M. & Dodson, E. (2003). A graphical user interface to the CCP4 program suite. *Acta Crystallogr. Sect. D: Biol. Crystallogr.* **59**, 1131–1137.
37. Storoni, L., McCoy, A. & Read, R. (2004). Likelihood-enhanced fast rotation functions. *Acta Crystallogr. Sect. D: Biol. Crystallogr.* **60**, 432–438.
38. Brünger, A., Adams, P., Clore, G., DeLano, W., Gros, P., Grosse-Kunstleve, R. *et al.* (1998). Crystallography and NMR system: a new software suite for macromolecular structure determination. *Acta Crystallogr. Sect. D: Biol. Crystallogr.* **54**, 905–921.
39. Brünger, A. (1993). Assessment of phase accuracy by cross validation: the free *R* value. Methods and applications. *Acta Crystallogr. Sect. D: Biol. Crystallogr.* **49**, 24–36.
40. Jones, T., Zou, J., Cowan, S. & Kjeldgaard, M. (1991). Improved methods for building protein models in electron density maps and the location of errors in these models. *Acta Crystallogr. Sect. A*, **47 (Pt 2)**, 110–119.
41. Kleywegt, G. J. (1996). Use of non-crystallographic symmetry in protein structure refinement. *Acta Crystallogr. Sect. D: Biol. Crystallogr.* **52**, 842–857.
42. Kabsch, W. & Sander, C. (1983). Dictionary of protein secondary structure: pattern recognition of hydrogen-bonded and geometrical features. *Biopolymers*, **22**, 2577–2637.
43. Krissinel, E. & Henrick, K. (2004). Secondary-structure matching (SSM), a new tool for fast protein structure alignment in three dimensions. *Acta Crystallogr. Sect. D: Biol. Crystallogr.* **60**, 2256–2268.
44. Uchiyama, T., Miyoshi-Akiyama, T., Kato, H., Fujimaki, W., Imanishi, K. & Yan, X. J. (1993). Superantigenic properties of a novel mitogenic substance produced by *Yersinia pseudotuberculosis* isolated from patients manifesting acute and systemic symptoms. *J. Immunol.* **151**, 4407–4413.

INFECTION AND IMMUNITY, Apr. 2007, p. 1721–1729 Vol. 75, No. 4
0019-9567/07/$08.00+0 doi:10.1128/IAI.01183-06

Cloning, Expression, and Characterization of the Superantigen Streptococcal Pyrogenic Exotoxin G from *Streptococcus dysgalactiae*[∇]

Jizi Zhao,[1,2]† Tomohito Hayashi,[3] Susanna Saarinen,[4] Anastassios C. Papageorgiou,[4] Hidehito Kato,[2] Ken'ichi Imanishi,[2] Teruo Kirikae,[1] Ryo Abe,[3] Takehiko Uchiyama,[2] and Tohru Miyoshi-Akiyama[1]*

Department of Infectious Diseases, Research Institute, International Medical Center of Japan, 1-21-1, Toyama, Shinjuku-ku, Tokyo 162-8655, Japan[1]; Department of Microbiology and Immunology of Tokyo Women's Medical University, 8-1 Kawada-cho, Shinjuku-ku, Tokyo 162-8666, Japan[2]; Division of Immunobiology, Research Institute for Biological Science, Tokyo University of Science, 2641, Yamasaki, Noda, Chiba 278-8510, Japan[3]; and Turku Centre for Biotechnology, University of Turku, Turku 20521, Finland[4]

Received 27 July 2006/Returned for modification 10 August 2006/Accepted 24 December 2006

We identified seven novel variants of streptococcal pyrogenic exotoxin G (SPEGG), a superantigen, in *Streptococcus dysgalactiae* subsp. *dysgalactiae* or *equisimilis* isolates from clinical cases of infection in humans and animals. Phylogenetic analysis of the SPEGG variants indicated two clades in the dendrogram: one composed of variants derived from the bacteria isolated from the humans and the other composed of variants from the bacteria isolated from the animals. Bovine peripheral blood mononuclear cells (PBMCs) were stimulated effectively by recombinant SPEGGs (rSPEGGs) expressed in *Escherichia coli*, while human PBMCs were not stimulated well by any of the rSPEGGs tested. SPEGGs selectively stimulated bovine T cells bearing Vβ1,10 and Vβ4. Bovine serum showed reactivity to the rSPEGG proteins. These results indicated that SPEGGs have properties as superantigens, and it is likely that SPEGGs play a pathogenic role in animals.

Bacterial superantigens (SAGs) bind simultaneously to major histocompatibility complex (MHC) class II molecules on antigen-presenting cells and T-cell receptor (TCR) molecules, and binding leads to the stimulation of large numbers of T cells in a TCR β-chain Vβ-selective manner. *Streptococcus pyogenes* (group A *Streptococcus* [GAS]), *Staphylococcus aureus*, *Yersinia pseudotuberculosis*, and *Mycoplasma arthritidis* are known as SAG producers (1, 18, 37). Overactivation of T cells by SAGs has been implicated in the pathogenesis of infectious diseases, such as toxic shock syndrome (TSS) and neonatal TSS-like exanthematous disease, as well as systemic *Yersinia pseudotuberculosis* infection.

It has been proposed that allelic variation in human leukocyte class II antigens affects the severity of invasive streptococcal infections, including streptococcal TSS (STSS) by regulating cytokine responses to streptococcal SAGs (17). However, we found that GAS isolated from STSS cases produced smaller amounts of SAGs than did GAS isolated from non-STSS cases (21). Most SAGs have highly conserved secondary and tertiary structures despite minimal amino acid sequence homology. Some SAGs, such as SMEZ (28), staphylococcal enterotoxin C (SEC), SPE-A (16, 22), SPE-G and SSA (30), and *Y. pseudotuberculosis*-derived mitogen show allelic variations, which are characterized by single- or multiple-amino-acid replacement.

In addition to GAS, serological group C and G streptococci possess genes that encode molecules similar to SAGs. For example, *S. dysgalactiae* subsp. *dysgalactiae* produces *S. dysgalactiae*-derived mitogen (SDM) (20). *S. equi*, the cause of equine strangles, produces *S. equi* pyrogenic exotoxin H (SePE-H), SePE-I, SPE-L_{Se}, and SPE-M (3, 29). Recently, there have been a number of clinical case reports of STSS caused by *S. dysgalactiae* subsp. *equisimilis*, though *S. dysgalactiae* strains are generally pathogenic in animals (4, 8, 12, 15, 19, 25, 26, 38). In addition to SDM, *S. dysgalactiae* harbors a gene encoding a protein similar to SPE-G, which has been designated in different ways, such as *spegg* or *speG*^{dys} (7, 11, 31). Here, we use "*spegg*" for the gene. Hashikawa et al. analyzed the prevalence of SAGs in 12 clinical isolates of *S. dysgalactiae* from STSS cases by PCR and found that only *spegg* was detected in 7 isolates, with none of the other superantigen genes being detected in any of the strains (11). Brandt et al. analyzed the mitogenic activity of *S. dysgalactiae* isolates carrying *spegg* and found no mitogenic activity in culture supernatants (7). However, there have been no previous studies of the biological properties of the *spegg* gene products. In this study, we analyzed the prevalence of *spegg* in *S. dysgalactiae* isolates from humans and animals and analyzed their biological activities using recombinant proteins encoded by the *spegg* genes. We also performed molecular modeling analysis to examine the point mutations found in SPEGG variants.

MATERIALS AND METHODS

Bacterial strains and growth conditions. All *S. dysgalactiae* isolates used in this study were isolated from human subjects or animals. Individual strains were stored in brain heart infusion (BHI) broth (Difco, Franklin Lakes, NJ) containing 7% dimethyl sulfoxide at −80°C until use. They were cultured overnight in BHI broth at 37°C in a humidified 5% CO_2 incubator as described previously (21). For expression of the six-His (His_6)-tagged proteins, *Escherichia coli*

* Corresponding author. Mailing address: Department of Infectious Diseases, Research Institute, International Medical Center of Japan, 1-21-1, Toyama, Shinjuku-ku, Tokyo 162-8655, Japan. Phone: 81-3-3202-7181, ext. 2903. Fax: 81-3-3202-7364. E-mail: takiyam@ri.imcj.go.jp

† Present address: Department of Special Pathogens, International Research Center for Infectious Disease, Research Institute for Microbial Disease, Osaka University, 3-1, Yamadoka, Suita, 565-0875, Osaka, Japan.

∇ Published ahead of print on 5 February 2007.

TABLE 1. *Streptococcus dysgalactiae* isolates used in this study

Strain	Group	*S. dysgalactiae* subsp.	Hemolysis type	Origin	*emm* type	SPEGG	Accession no.	Gene name deposited in database
125	C	*equisimilis*	β	Human	*stg653*	–		
152	C	*equisimilis*	β	Human	–	–		
154	C	*equisimilis*	β	Human	–	–		
164	G	*equisimilis*	β	Human	*stg485*	SPEGG2	AB105080	*spegg4*
162	C	*equisimilis*	β	Human	–	–		
160	G	*equisimilis*	β	Human	*stg652*	–		
163	G	*equisimilis*	β	Human	*stg643*	–		
167	C	*equisimilis*	β	Human	*stL839*	SPEGG3	AB105081	*spegg5*
165	G	*equisimilis*	β	Human	–	–		
168	G	*equisimilis*	β	Human	ND[a]	SPEGG4	AB105078	*spegg2*
169	G	*equisimilis*	β	Human	*stg11*	SPEGG3		
170	G	*equisimilis*	β	Human	ND	SPEGG5	AB105079	*spegg3*
1586	G	*equisimilis*	β	Human	*stc36*	SPEGG5		
1149	G	*equisimilis*	β	Human	ND	+		
1317	G	*equisimilis*	β	Human	ND	+		
1379	G	*equisimilis*	β	Human	*Stg4831*	+		
1434	G	*equisimilis*	β	Human	*Stg2028*	+		
1412	G	*equisimilis*	β	Human	*Stg485*	SPEGG2		
8	C	*equisimilis*	α	Cow	–	–		
9	C	*equisimilis*	β	Cow	ND	SPEGG6	AB105077	*spegg1*
62	C	*equisimilis*	β	Cow	*stL2764*	–		
63	C	*equisimilis*	β	Cow	–	–		
64α	C	*equisimilis*	β	Cow	–	–		
64β	C	*equisimilis*	β	Cow	*stL2764*	–		
65	C	*dysgalactiae*	β	Cow	*stL2764*	–		
10	C	*dysgalactiae*	α	Cow	–	–		
12	C	*dysgalactiae*	α	Cow	–	–		
SD-1	C	*dysgalactiae*	β	Animal	–	SPEGG7	AB105083	*spegg7*
SD-2	C	*dysgalactiae*	β	Animal	*stL2764*	–		
SD-3	C	*dysgalactiae*	β	Animal	–	SPEGG7		
SD-4	C	*dysgalactiae*	β	Animal	–	–		
SD-5	C	*dysgalactiae*	β	Animal	–	–		
SD-6	C	*dysgalactiae*	β	Animal	*stL2764*	SPEGG8	AB105084	*spegg8*
SD-7	C	*dysgalactiae*	β	Animal	*stL2764*	SPEGG7		
16008sα-8	C	*dysgalactiae*	β	Animal	*stL2764*	–		
16009sα-9	C	*dysgalactiae*	β	Animal	*stL2764*	–		
SD-10	C	*dysgalactiae*	β	Animal	–	–		
SD-11	C	*dysgalactiae*	α	Animal	–	–		
16021	C	*dysgalactiae*	α	Animal	–	–		
124	G	*equisimilis*	β	Animal	*stg2028*	–		
151	C	*dysgalactiae*	β	Animal	–	–		

[a] ND, sequencing analysis was not done because of the presence of multiple amplicons.

M15(pREP4) (QIAGEN, Tokyo, Japan) was used for transformation with expression constructs derived from pQE30 (QIAGEN).

Preparation of genomic DNA and *emm* typing. Chromosomal DNA was prepared from the *S. dysgalactiae* isolates as described previously (20). Briefly, bacteria grown in BHI broth overnight were collected and lysed by serial treatment with mutanolysin (Sigma-Aldrich, Tokyo, Japan), lysozyme, freeze-thaw cycling, and proteinase K (Sigma-Aldrich). *S. dysgalactiae* isolates were subjected to *emm* typing as described previously (http://www.cdc.gov/ncidod/biotech/strep/M-ProteinGene_typing.htm) (21). Briefly, genomic DNA from *S. dysgalactiae* was used as the template for PCR using specific primers A (5′-TATTAGCTTAGAAAATTAA-3′) and B (5′-GCAAGTTCTTCAGCTTGTTT-3′). The resulting PCR fragments were sequenced with a Genetic Analyzer 310 system (Applied Biosystems, Tokyo, Japan).

PFGE. Large restriction fragment profiles of all of the isolates were obtained by SmaI digestion followed by pulsed-field gel electrophoresis (PFGE) as described previously (21). Briefly, plugs prepared from the isolates were treated sequentially with achromopeptidase, RNase, lysozyme, mutanolysin, sodium deoxycholate, sodium laurylsarcosine, Brij-58, EDTA, and proteinase K. After digestion with SmaI, the plugs were electrophoresed in a Genepath contour-clamped homogeneous electric field apparatus (Bio-Rad Labs, Tokyo, Japan) and the patterns were analyzed with Molecular Analyst Fingerprinting Plus software, version 1.6 (Bio-Rad Laboratories, Inc., Hercules, CA).

Amino acid sequence alignment and dendrogram preparation. The *spegg* genes from *S. dysgalactiae* genomic DNA in Table 1 were amplified using several combinations of the primers listed in Table 2 and ExTaq (Takara, Shiga, Japan), because the sequences of *spegg* including the proximal region were different in several clinical isolates. The PCR products were sequenced directly after purification with a QIAquick PCR purification kit (QIAGEN). The SPEGG amino acid sequences were aligned with those of known bacterial SAGs, and a dendrogram was constructed using the search and analysis service based on Clustal W at DDBJ (http://www.ddbj.nig.ac.jp). The dendrogram was drawn using the TreeView program (27).

Expression and purification of rSPEGG. DNA fragments encoding the mature form of SPEGG, as speculated from the cleavage site of signal sequence in SPE-G (accession no. AAF60291), were amplified by PCR. Because there was sequence variation among *spegg* subtypes, two primers containing a BamHI or SalI site were chosen from the list of primers in Table 2. The fragments were amplified and cloned with a TOPO-TA cloning kit (Invitrogen) and then sequenced and subcloned in the corresponding restriction sites of pQE30 (QIAGEN). The resulting pQE30 derivatives were transformed into *E. coli*. Induction with isopropyl-thio-β-D-galactopyranoside resulted in production of His_6-tagged recombinant SPEGGs (rSPEGGs). The His_6-tagged proteins were purified by chromatography with chelating Sepharose 4B (Amersham Pharmacia Biotech) preloaded with Ni^{2+} according to the manufacturer's instructions.

TABLE 2. Primers used in this study

Primer name (direction)[a]	Sequence[b]
A (forward)	TATTAGCTTAGAAAATTAA
B (reverse)	GCAAGTTCTTCAGCTTGTTT
G1 (forward)	TTAAG**GATCC**GATGAAATATTAAAAGATTTG
G2 (reverse)	CGCC**GTCGAC**CTAGTGCGTTTTTAAGTAGAT
G3 (forward)	AAGCCCTTGCAAATGCATCA
G4 (forward)	CCTTTATGAACTTCCTCACT
G5 (reverse)	TGATTAACTCGACACCAATC
G6 (reverse)	AATCTACAGGCGAGCCATGA
G7 (forward)	TTAAG**GATCC**GATGAAATATCAAAAGATTTG
G8 (forward)	TTAAG**GATCC**GATGAAATATTAAATGATTTG
G9 (forward)	TTAAG**GATCC**GATGAAATATTAAAAGATTTG
G10 (reverse)	CGCC**GTCGAC**CTAGTGTGTTTTTAAGTAGAT
G11 (reverse)	CGCC**GTCGAC**CTAGTGCGTTTTTAAGTAGAT
G12 (reverse)	CGCC**GTCGAC**CTAGTGTGTTTTTAAGTAGAC

[a] Primers A and B for *emm* typing were designed according to the previous description (http://www.cdc.gov/ncidod/biotech/strep/M-ProteinGene_typing.htm). Primers G1 to G12 were designed based on the sequence of accession no. AJ489606.

[b] The sequences for recognition by the restriction enzymes are indicated in boldface.

Human and bovine PBMC proliferation assays and bovine T-cell repertoire analysis. Bovine and human peripheral blood mononuclear cells (PBMCs) were prepared as described previously (23, 36). Briefly, human or bovine PBMCs were obtained from healthy donors and separated by Ficoll-Conray density gradient centrifugation. T-cell-depleted bovine PBMCs were prepared by cell sorting of cells negative for CD2, CD4, and CD8 using an EPICS ALTRA cell sorter (Beckman-Coulter, Fullerton, CA). Purified PBMCs of human, bovine (1×10^5 cells/well), and bovine T-cell-depleted populations in 96-well plates were stimulated with rSPEGG2 to rSPEGG8 or SPE-G. Primary proliferative response was measured by [^{3}H]thymidine uptake assay. Analysis of the Vβ repertories of bovine T cells stimulated by SPEGG was performed as described previously (23). Briefly, bovine PBMCs were incubated with recombinant proteins (1 μg/ml) at 10^5 cells/well for 3 days, and mRNAs were prepared using ISOGEN (Nippon Gene, Tokyo, Japan) from the induced T-cell blasts. cDNAs synthesized from the mRNA samples by avian myeloblastosis virus reverse transcriptase XL with random DNA hexamers (Takara, Shiga, Japan) were used as templates for PCR amplification of each Vβ fragment using *Taq* DNA polymerase (Sigma-Aldrich) with 26 5′ Vβ-specific primers and a 3′-Cβ-specific antisense primer.

Reactivity of bovine serum to the rSPEGG proteins. To detect antibodies reactive to SPEGG in bovine serum, a conventional enyzyme-linked immunosorbent assay (ELISA) was performed. Briefly, each well in Maxisorp ELISA plates (Nunc, Rochester, NY) was filled with 50 μl of rSPEGG solution (1 μg/ml in 50 mM $Na\text{-}CO_3$ [pH 9.0]) and incubated for 1 h at room temperature. After blocking the wells with SuperBlock (Pierce, Rockford, IL), the wells were incubated with 1:1,000-diluted bovine serum samples for 1 h at room temperature. After washing the wells, antibodies reactive with the rSPEGGs were detected with horseradish peroxidase-labeled anti-goat immunoglobulin G, which cross-reacts with bovine immunoglobulin G (Biosource Camarillo, CA).

Homology modeling. Models of SPEGG based on SPEGG2 and SPEGG3 sequences were made based on the SPE-C structure (PDB entry 1AN8) using the program MODELLER (32).

Nucleotide sequence accession number. The DNA sequences for *spegg2* to *spegg8* have been deposited in the DDBJ under the accession numbers listed in Table 1.

RESULTS

Distribution of *spegg* in *S. dysgalactiae*. We screened 41 independent isolates of *S. dysgalactiae* subsp. *dysgalactiae* (GCS) or *S. dysgalactiae* subsp. *equisimilis* (GCS or GGS) from the humans or animals by PCR with *spegg*-specific primers (G1 and G2; Table 2). Sixteen of the 41 (39%) *S. dysgalactiae* isolates tested positive for *spegg*. Nineteen M/*emm* types were detected among the *S. dysgalactiae* isolates, although the *emm* gene was not amplified in 22 isolates with the primer pair used. The *emm* types of the *S. dysgalactiae* isolates carrying *spegg* genes were *stg485*, *stL839*, *stg11*, *stc36*, *stg485*, *stL2764*, *stg4831*, *stg2028*, and *stg6*, respectively. Several reports suggested that types of SPE in GAS strains correlate with their *emm* types (28). However, in the present study, the *emm* type did not correlate with the prevalence of *spegg* in *S. dysgalactiae*, in accordance with reports of *S. dysgalactiae* isolates from human subjects (11). PFGE analysis was performed with the isolates after SmaI digestion, and the PFGE profiles were found to vary among the isolates regardless of the presence of *spegg* (Fig. 1). PFGE profiles also varied among isolates carrying the same *spegg* variant, except for strains 170 and 1586, both of which carry *spegg5*. Although the prevalence of *spegg* was higher in the isolates from humans than in those from animals, *spegg* was not detected in some of the human isolates, such as 154, 152, and 162.

Sequence variation of *spegg*. Although the presence of *spegg* in *S. dysgalactiae* has been reported (7, 11, 31), characterization of the SPEGG protein encoded by the *spegg* gene has not been performed. To investigate the possibility that *spegg* exhibits allelic variations, such as SPE-A and SMEZ, we sequenced 12 of the 16 *spegg* genes detected in this study (Table 1) and identified 7 different alleles based on the sequences within the open reading frames. None of the genes in the isolates examined in this study were identical to *spegg1* reported previously (accession no. AJ294849). SPEGGs showed about 84% similarity to SPE-G. Forty-one mutations were detected at the DNA sequence level. Most of the changes were A/G (31.7%), T/C (19.5%), C/A (9.7%), and T/C (9.7%) transitions, while G/C translation occurred only at position 169. Eighteen of the variable positions resulted in amino acid changes, while the others were synonymous mutations. Interestingly, the positions of the SPEGG mutations in *S. dysgalactiae* isolates from humans were clearly different from those in isolates from animals, except for mutations at amino acid positions 4, 5, and 8 (IK.K) and 98 and 99 (KL or KH), which were found in both the human and animal isolates (Fig. 2). Because the mutations at amino acid positions 4, 5, and 8 are located in the putative signal peptide sequence, they do not seem to affect function when they are expressed.

As expected from the sequence similarity, phylogenetic analysis of the SAGs indicated that SPEGGs were related to SPE-G (Fig. 3). There are three major clades in the phylogenetic tree: clades I and II are comprised of GAS, GCS, GGS, and staphylococcal SAGs, while clade III contains only streptococcal SAGs, including SPEGGs. In clade III, SPEGG variants are clearly divided into two subgroups: those in the animal isolates (SPEGG6 to SPEGG8 [SPEGG animal forms]) and those in the human isolates (SPEGG2 to SPEGG5 [SPEGG human forms]).

Comparison of SAG activities of rSPEGGs and SPE-G on human and bovine PBMCs. To determine whether SPEGG has SAG properties, we first analyzed the mitogenic activities of the culture supernatants from the *S. dysgalactiae* isolates. However, we did not detect any mitogenic activities in any of the isolates tested (data not shown), which may be due to the lack of expression of *spegg* under the bacterial culture conditions used. Therefore, all variants of SPEGGs were expressed in *E. coli* as recombinant proteins to analyze further their

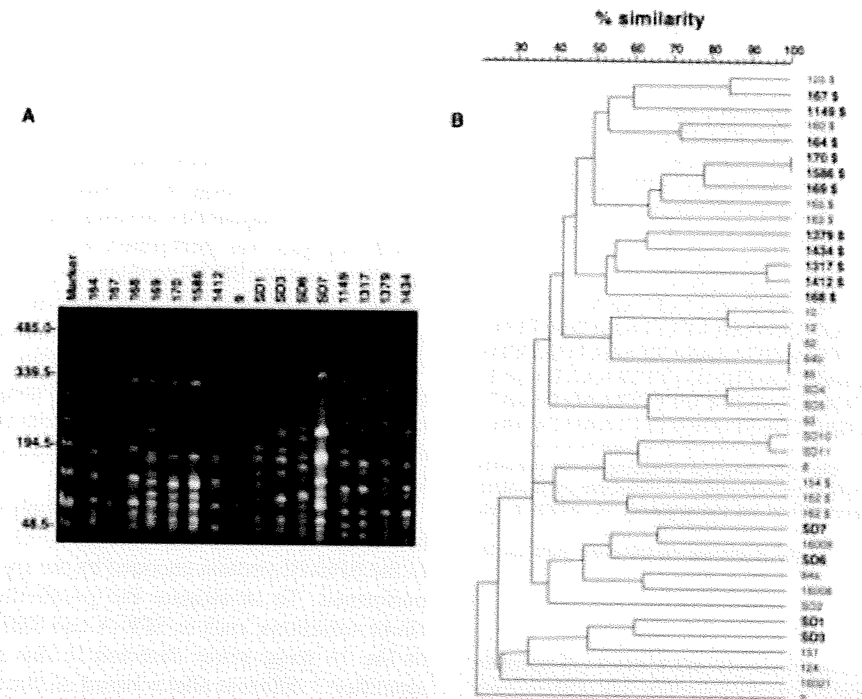

FIG. 1. PFGE pattern of *S. dysgalactiae* isolates carrying *spegg* genes and a dendrogram constructed by computer-assisted comparison of PFGE patterns generated from all isolates used in this study. In the dendrogram, the isolates carrying *spegg* are shown in boldface. Isolates from humans are indicated with a dollar sign ($). The scale bar indicates percent similarity among the isolates.

function as SAGs and to determine whether their function was affected by the mutations. rSPEGGs were used to stimulate human or bovine PBMCs, and [^{3}H]thymidine uptake by the cells was measured to analyze their proliferation. Proliferation of bovine PBMCs was induced by the animal forms SPEGG6, SPEGG7, and SPEGG8 at a dose of 0.01 ng/ml, while induction of bovine PBMC proliferation by the human forms, SPEGG2 to SPEGG5, required concentrations of 0.1 ng/ml (Fig. 4). Among the human forms, only SPEGG2 showed higher activity than SPEGG3, SPEGG4, and SPEGG5 against bovine PBMCs. In contrast, concentrations of 100 ng/ml or more of the proteins were required to induce proliferation of human PBMCs. T-cell-depleted bovine PBMCs did not respond to any of the SPEGGs. These findings indicated that

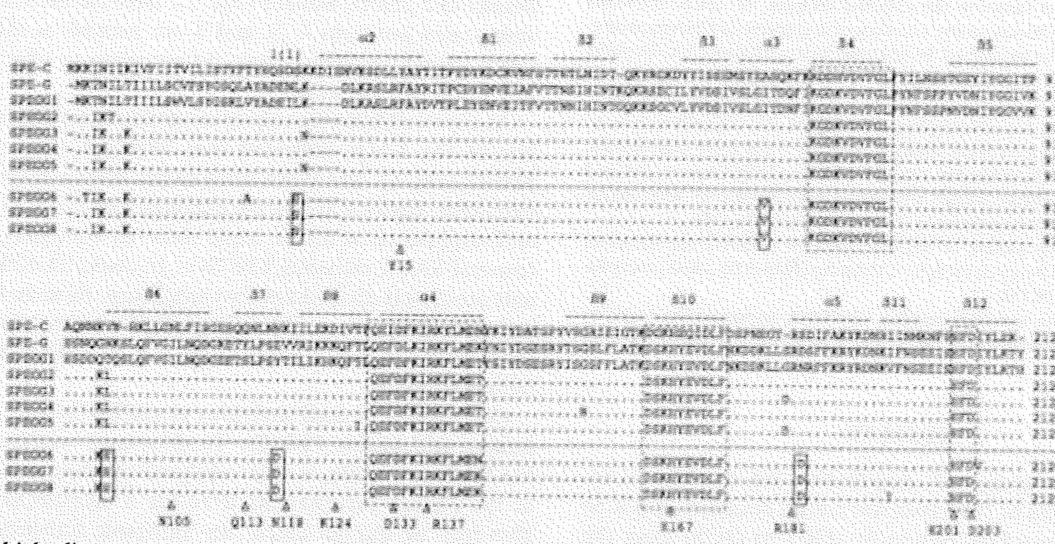

FIG. 2. Multiple alignment of SPE-C, SPE-G, and SPEGG amino acid sequences. The amino acid sequences were aligned using Clustal W (35). The bars above the sequences indicate the secondary structure based on the crystal structure of SPE-C (PDB identification no. 1AN8). Highly conserved regions and the zinc-binding motif are boxed with dotted lines. SPEGG variants derived from isolates from animals (SPEGG6 to SPEGG8) are separated with a dotted line from those from humans, and the residues commonly mutated in SPEGG6 to SPEGG8 are indicated in boxes (also see Fig. 6). Corresponding residues of interest (see text for details) in the alignment are marked with Δ.

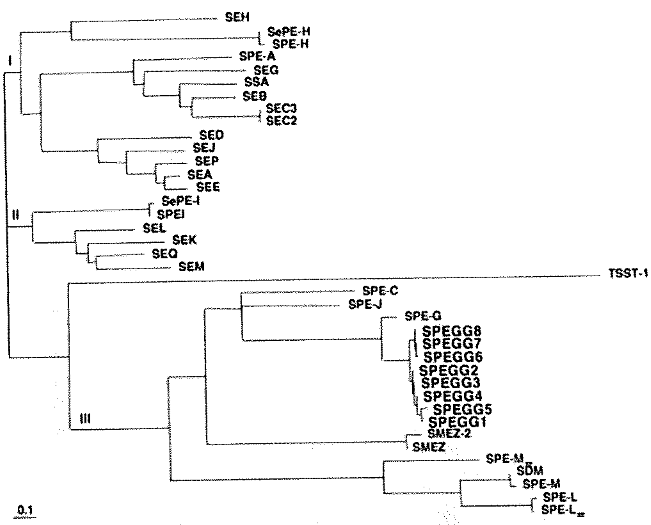

FIG. 3. Phylogenetic tree of streptococcal and staphylococcal SAGs, including SPEGGs. This phylogenetic tree was constructed using Clustal W, and the GenBank accession numbers of the SAGs sequences are as follows: SEH, CAI77677; SePE-H, AAF72809; SPE-H, AAK33907; SPE-A, AAL97141; SEG, AAX11325; SSA, AAA65928; SEB, AAL04126; SEC3, AAA26624; SEC2, P34071; SED, P20723; SEJ, AAC78590; SEP, BAB43036; SEA, AAP37183; SEE, P12993; SePE-I, AAF72808; SPE-I, AAL31571; SEL, BAB58170; SEK, AAL04147; SEQ, AAL04146; SEM, AAG36925; TSST-1, BAB58173; SPE-C, AAA27017; SPE-J, AAZ50974; SPE-G, AAZ50801; SMEZ-2, AAD52087; SMEZ, CAD91900; SPE-L, BAC63752; SPE-Lse, CAH65000; SPE-Mse, CAH68555; SPE-M, AAL97849; and SDM, AB074529.

SPEGG animal forms can stimulate bovine PBMCs more effectively than the human forms and that stimulation of bovine PBMCs occurs in a T-cell-dependent manner.

Identification of TCR Vβ repertories of bovine T cells reactive to rSPEGGs. As SPEGG showed T-cell-dependent PBMC stimulation, we next performed reverse transcription-PCR analyses to characterize the Vβ repertories of bovine T cells reactive to SPEGG (Table 3). The Vβ profiles of bovine PBMCs stimulated with rSPEGGs were compared with those stimulated with concanavalin A (ConA) and SPE-G (cow 1 in experiment 1), staphylococcal enterotoxin B (SEB) (cow 2 in experiment 2), or SPE-G (cow 3 in experiment 3). Blasts induced by stimulation with SPEGG2, SPEGG6, SPEGG7, SPEGG8, and SPE-G were significantly richer (two- to sevenfold) in Vβ1,10 and Vβ4 than those stimulated with ConA or SEB (experiment 1). Blasts induced by rSPEGG2, -3, and -6 were slightly richer (about twofold) in Vβ50 in cow 1 but not in cows 2 and 3. Blasts induced by rSPEGG3 and 5 were similar in Vβ50 to those induced by SPE-G in cow 1 but not in cows 2 and 3. These experimental variations might come from individual differences in the responses of T cells in cattle. There were more blasts with Vβ1,10 than with other Vβs, especially in experiments 2 and 3, suggesting that the T cells most reactive to SPEGGs were those with Vβ1,10. These results indicated that T-cell blasts induced by SPEGGs showed a bias in the Vβ repertoire, suggesting that SPEGGs act as SAGs on bovine T cells.

Recognition of rSPEGGs by bovine immune system. There have been no reports of the expression of *spegg* in *S. dysgalac-*

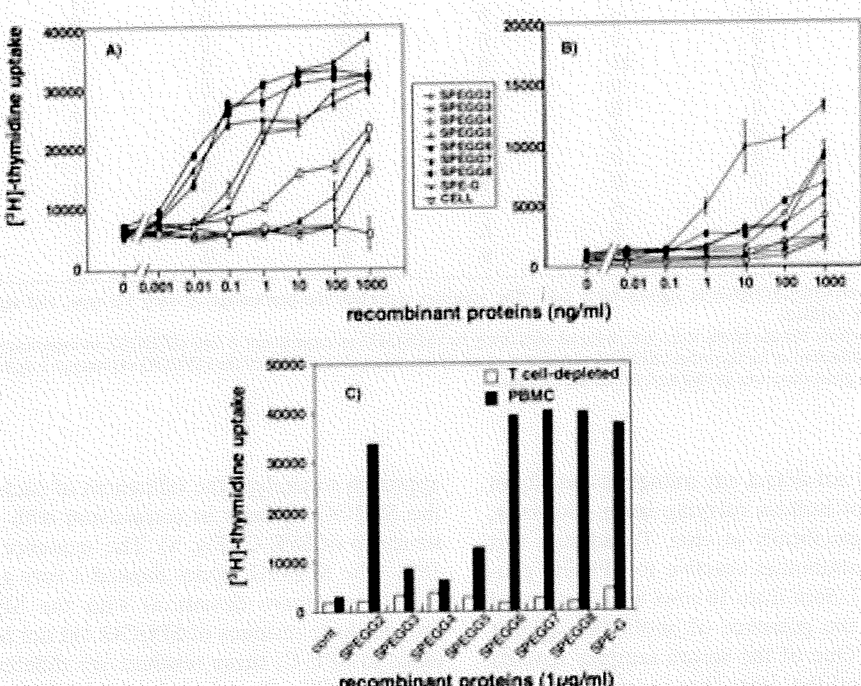

FIG. 4. Stimulation of human and bovine PBMCs with rSPEGGs. PBMCs were isolated from bovine (A) and human (B) blood samples and incubated with various concentrations of rSPEGGs. After 2 days, 0.1 μCi of [^{3}H]thymidine was added, and cells were incubated for a further 18 h before being harvested and counted for the thymidine uptake with a beta counter. These experiments are representative of four independent experiments. In panel C, bovine PBMCs (solid bars) and T-cell-depleted bovine PBMCs (open bars) were stimulated with 1 μg/ml of SPEGGs and SPE-G for 2 days and the mitogenic response was measured as described in Materials and Methods. Serial dilution was performed without SPEGG and used as a negative control (marked as "cell"). cont, control.

TABLE 3. TCR Vβ repertories of bovine T cells stimulated with rSPEGG and SPE-G

Bovine Vβ type	% of Vβ type induced when stimulated by[a]:									
	ConA	SEB	rSPEGG2[b]	rSPEGG3[b,c]	rSPEGG4[c]	rSPEGG5[c]	rSPEGG6	rSPEGG7	rSPEGG8	SPE-G
Expt 1										
1,10	16		**17**	9	0	**18**	**41**	0	**31**	**26**
4	15		13	8	0	15	**40**	0	**32**	**24**
13	2		0	0	0	4	0	0	0	0
13C	0		0	0	0	0	0	0	0	0
18	13		13	0	0	5	3	0	0	2
22	0		0	0	0	0	0	0	0	0
27	13		**19**	**26**	0	**29**	3	0	**16**	**24**
35,91	3		0	0	0	0	0	0	0	0
45	0		0	0	0	0	0	0	0	0
50	6		**15**	**17**	0	6	4	0	1	0
82C	3		6	3	0	2	2	0	2	0
90	18		17	**36**	0	**21**	5	0	17	**24**
93	12		0	0	0	0	3	0	0	0
Expt 2										
1,10		**11**	**52**	0	0	0	**49**	**79**	**54**	
4		9	**48**	0	0	0	**39**	**21**	**41**	
13		0	0	0	0	0	0	0	0	
13C		0	0	0	0	0	0	0	0	
18		**10**	0	0	0	0	5	0	0	
22		8	0	0	0	0	0	0	0	
27		9	0	0	0	0	0	0	0	
35,91		0	0	0	0	0	0	0	0	
45		**13**	0	0	0	0	0	0	0	
50		0	0	0	0	0	0	0	0	
82C		0	0	0	0	0	0	0	5	
90		**40**	0	0	0	0	4	0	0	
93		0	0	0	0	0	0	0	0	
Expt 3										
1,10			0	**52**	0	0	**100**	**85**	**100**	**39**
4			0	**16**	0	0	0	**12**	0	**27**
13			0	0	0	0	0	0	0	0
13C			0	0	0	0	0	0	0	0
18			0	**21**	0	0	0	0	0	8
22			0	0	0	0	0	0	0	0
27			0	0	0	0	0	0	0	**14**
35,91			0	0	0	0	0	0	0	0
45			0	0	0	0	0	0	0	0
50			0	0	0	0	0	0	0	9
82C			0	6	0	0	0	1	0	0
90			0	5	0	0	0	2	0	2
93			0	0	0	0	0	0	0	1

[a] Bovine PBMCs were incubated with rSPEGGs (1 μg/ml) for 3 days. The numbers represent the percentage of each Vβ type, and significant responses in the rSPEGG variants are indicated in boldface.

[b] Because of experimental variation, bovine blasts were not induced effectively by rSPEGG2 in experiment 3 and rSPEGG3 in experiment 2.

[c] Induction of blasts was not as effective as for the other rSPEGG variants because of low mitogenic activity of the rSPEGG variants at 1 μg/ml against bovine PBMCs, although the entire experimental procedure was performed for those variants.

tiae isolates, and we could not detect any mitogenic activity in the culture supernatants of isolates carrying *spegg*. However, *spegg* may be expressed specifically in vivo. To address this possibility, we quantified antibodies reactive to SPEGG proteins in bovine sera (Fig. 5). Sera from 10 cows were incubated with rSPEGGs to detect the presence of antibodies against these proteins in ELISA. One of the serum samples reacted strongly to all SPEGGs, and the other three samples reacted with SPEGG3, indicating that a certain proportion of the cattle had been exposed to SPEGG.

Structural comparison of SPEGG based on homology modeling. As the SPEGG variants showed marked differences with regard to mitogenic activity, we used a molecular modeling approach to analyze the influences of each mutation found in the SPEGG variants in comparison with the known tertiary structure of SPE-C (Fig. 6). The sequence identity was about 38%. The SPEGG model showed a very good match (0.28-Å root-mean-square deviation) with the SPE-C structure, although three residues of SPEGG did not have equivalent residues in SPE-C; these residues are different in the sequence alignment (Fig. 2) and in the model. These discrepancies are probably due to the difference in the methodologies of the alignment analysis and the modeling approach.

Residues needed for intramolecular hydrogen bonds combining N and C domains in SPE-C are conserved in SPEGG, and their positions are structurally very similar to those

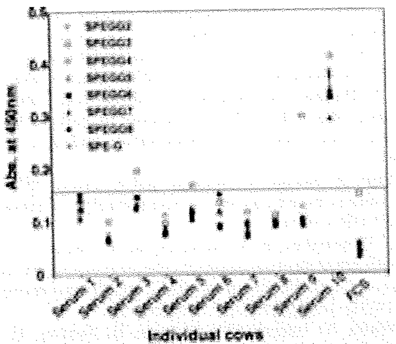

FIG. 5. Reactivity of bovine serum to rSPEGGs. Serum samples obtained from 10 cows were diluted 1:1,000, and their reactivity to SPEGG was analyzed using ELISA. Fetal calf serum (FCS) was used as a negative control, and the threshold line is presented according to the absorbance (Abs.) obtained from FCS.

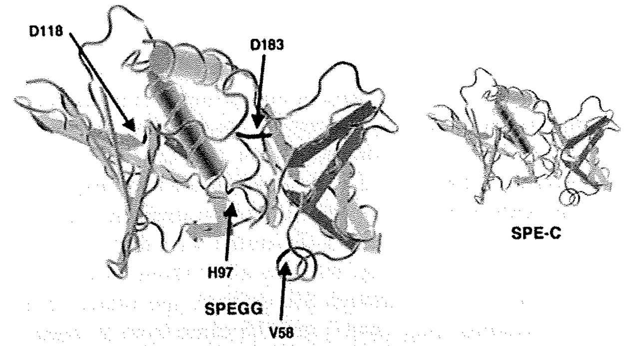

FIG. 6. Molecular modeling of the SPEGG protein. SPEGG2 and -3 were modeled onto the crystal structures of SPE-C with MODELLER (32). Residues that differed between animal and human forms of SPEGG are shown in black.

in SPE-C (2). Salt bridge formation between Asp133 and Arg137 (SPE-C numbering) is also possible in SPEGG. Lys124 in SPE-C is superimposed on His of SPEGG, and this could be a difference between SPEGG and SPE-G because SPE-G has Lys, similar to SPE-C. SPE-C Lys124 forms a salt bridge with SPE-C Glu131. His is also a positively charged residue that can form salt bridges, but the distance between His and Glu can be longer in SPEGG than in SPE-C.

The zinc-binding residues of SPE-C (His167, His201, and Asp203 in SPE-C), which are necessary to provide a binding site for MHC class II in a zinc-dependent manner, are also conserved in SPEGG and SPE-G. MHC class II binding of SPE-G shows clear zinc dependency, and it seems that SPEGG could act in the same way. There is some variation between SPE-C and SPEGG sequences in the residues involved in MHC class II β-chain binding. SPE-C Asn105 (this Asn is conserved in other β-chain binding), which forms a hydrogen bond with MHC class II β-chain, is aligned and superimposed with Ile in SPEGG and SPE-G. Other residues involved in MHC class II binding are conserved, but neither SPEGG nor SPE-G has a residue similar to Gln113 of SPE-C, which is important for peptide binding.

On the other hand, there are clear differences between SPEGG and SPE-C in the residues involved in TCR binding, as judged from the SPE-C complex structures. The SPEGG residue equivalent to SPE-C Tyr15 (important for TCR binding) is replaced with Phe (also in SPE-G). Furthermore, in most cases, other SAGs have Asn in the same position and this residue is important for TCR binding. SPE-G and SPEGG must have some alternative way to bind TCR. Arg181 of SPE-C is another important residue for TCR binding, and both SPEGG and SPE-G have an equivalent Arg residue. Other residues of minor importance in TCR binding of SPE-C are dissimilar in SPEGG and SPE-G.

Taken together, the results of SPEGG modeling suggested strongly that there are some variations in MHC class II and TCR binding in comparison with SPE-C, but the sequence of SPEGG seems to fit the overall three-dimensional structure of SAG. The sequence variations among the SPEGGs probably have no direct effect on TCR or MHC class II binding because the variations are in regions peripheral to the putative binding sites for the MHC and TCR. Thus, the mechanism underlying the differences in mitogenic activities of SPEGG on bovine and human PBMCs and the differences in stimulation of bovine PBMCs between human and animal forms of SPEGG seem to be due to the differences in binding ability of human and bovine forms of SPEGG, which are affected indirectly by variations in the SPEGGs themselves.

DISCUSSION

In this study, we demonstrated that SPEGGs have mitogenic activity toward bovine PBMCs and also, to a lesser extent, toward human PBMCs. The mitogenic activity was dependent on the presence of the T-cell population in PBMCs, and SPEGG selectively activated bovine Vβ1,10- and Vβ4-positive T cells, strongly suggesting that SPEGGs act as SAGs.

Brandt et al. showed that *S. dysgalactiae* subsp. *equisimilis* clinical isolates from human invasive infections and from superficial infections lacked expression of *spegg* and had no mitogenic activity in their culture supernatants (7). As shown in this study, rSPEGG does not stimulate human PBMCs effectively. However, it stimulates bovine PBMCs effectively and a percentage of bovine sera contained antibodies reactive to SPEGG. These observations suggest that SPEGG has some pathogenic and/or physiological roles in cattle but not in humans. In addition, SPEGGs in animals seem to have been adapted to their environment, because all of the animal forms of SPEGG stimulated bovine PBMCs more effectively than the human forms. Igwe et al. reported that 10 of 20 *S. dysgalactiae* subsp. *equisimilis* isolates from the human invasive cases were positive for at least one SAG gene (13). Hashikawa et al. reported that 7 of 12 *S. dysgalactiae* subsp. *equisimilis* isolates from the human invasive cases were positive for *spegg* but none was positive for *speA*, *speC*, *speH*, *speI*, *speJ*, or *speL* (11). Brandt et al. reported that 6 of 46 *S. dysgalactiae* subsp. *equisimilis* isolates were positive for *spegg* but none was positive for *speA*, *speC*, *speH*, *speI*, *speJ*, *speK*, *speL*, *speM*, *smeZ*, or *ssa* (7). Due to the low prevalence and based on our analysis showing low mitogenic activity toward human PBMCs of rSPEGGs from bacteria isolated from the human STSS cases, SAGs of *S. dysgalactiae* seem to play very limited roles in the severity of invasive *S. dysgalactiae* subsp. *equisimilis* infection in humans.

Many SAGs have been shown to be located in the mobile genetic elements, such as defective prophages, active prophages, or bacteriophages, in the GAS genome (1, 14). These SAGs show sequence similarity to those of non-group A streptococci, suggesting that horizontal gene transfer has occurred between GAS and non-GAS. Such horizontal gene transfer may not be the case between SPEGG and SPE-G, which is a homologue of SPEGG in GAS. SPE-G is not located in any apparent mobile genetic elements in all of the GAS strains for which the genome sequences are available, whereas all of them have *speG* (5, 6, 9, 10, 24, 33, 34). Although Sachse et al. speculated that the region including *spegg* (*speG*) in GAS came from *S. dysgalactiae*, based on a comparison of the genomes of MGAS8232 and GAS SF370 (31), whole-genome data of the other GAS strains, such as MGAS10394 (accession no. NC_006086.1), which became available after their report, suggested that their speculation may not be true. Thus, the common ancestor of GAS and non-GAS may already have a common ancestor in SPEGGs and SPE-G instead of gene transfer among GAS and *S. dysgalactiae*. If this is true, SPEGG and SPE-G may be direct descendants of one of the ancestral SAGs of streptococci. Further genome-wide analyses of streptococci should provide the answers to these questions.

ACKNOWLEDGMENTS

The authors thank T. Fujino of the International Medical Center of Japan for excellent technical assistance.

This study was supported by a grant for research on emerging and reemerging infectious diseases (H12 Shinkou-27) from the Ministry of Health and Welfare, Japan. T. H. was supported by a High-Tech Research Center Project for Private Universities grant/matching-fund subsidy from the Ministry of Education, Culture, Sports, Science and Technology of Japan (MEXT), 2004–2008.

REFERENCES

1. **Alouf, J. E., and M. Popoff.** 2006. The comprehensive sourcebook of bacterial protein toxins, 3rd ed. Academic Press, San Diego, CA.
2. **Arcus, V. L., T. Proft, J. A. Sigrell, H. M. Baker, J. D. Fraser, and E. N. Baker.** 2000. Conservation and variation in superantigen structure and activity highlighted by the three-dimensional structures of two new superantigens from Streptococcus pyogenes. J. Mol. Biol. **299:**157–168.
3. **Artiushin, S. C., J. F. Timoney, A. S. Sheoran, and S. K. Muthupalani.** 2002. Characterization and immunogenicity of pyrogenic mitogens SePE-H and SePE-I of Streptococcus equi. Microb. Pathog. **32:**71–85.
4. **Assimacopoulos, A. P., J. A. Stoehr, and P. M. Schlievert.** 1997. Mitogenic factors from group G streptococci associated with scarlet fever and streptococcal toxic shock syndrome. Adv. Exp. Med. Biol. **418:**109–114.
5. **Banks, D. J., S. F. Porcella, K. D. Barbian, S. B. Beres, L. E. Philips, J. M. Voyich, F. R. DeLeo, J. M. Martin, G. A. Somerville, and J. M. Musser.** 2004. Progress toward characterization of the group A Streptococcus metagenome: complete genome sequence of a macrolide-resistant serotype M6 strain. J. Infect. Dis. **190:**727–738.
6. **Beres, S. B., G. L. Sylva, K. D. Barbian, B. Lei, J. S. Hoff, N. D. Mammarella, M. Y. Liu, J. C. Smoot, S. F. Porcella, L. D. Parkins, D. S. Campbell, T. M. Smith, J. K. McCormick, D. Y. Leung, P. M. Schlievert, and J. M. Musser.** 2002. Genome sequence of a serotype M3 strain of group A Streptococcus: phage-encoded toxins, the high-virulence phenotype, and clone emergence. Proc. Natl. Acad. Sci. USA **99:**10078–10083.
7. **Brandt, C. M., K. G. Schweizer, R. Holland, R. Lutticken, and B. S. Freyaldenhoven.** 2005. Lack of mitogenic activity of speG- and speG(dys)-positive Streptococcus dysgalactiae subspecies equisimilis isolates from patients with invasive infections. Int. J. Med. Microbiol. **295:**539–546.
8. **Eskens, F. A., P. E. Verweij, J. F. Meis, and A. Soomers.** 1995. Septic shock caused by group G beta-haemolytic streptococci as presenting symptom of acute myeloid leukaemia. Neth. J. Med. **46:**153–155.
9. **Ferretti, J. J., W. M. McShan, D. Ajdic, D. J. Savic, G. Savic, K. Lyon, C. Primeaux, S. Sezate, A. N. Suvorov, S. Kenton, H. S. Lai, S. P. Lin, Y. Qian, H. G. Jia, F. Z. Najar, Q. Ren, H. Zhu, L. Song, J. White, X. Yuan, S. W. Clifton, B. A. Roe, and R. McLaughlin.** 2001. Complete genome sequence of an M1 strain of Streptococcus pyogenes. Proc. Natl. Acad. Sci. USA. **98:** 4658–4663.
10. **Green, N. M., S. Zhang, S. F. Porcella, M. J. Nagiec, K. D. Barbian, S. B. Beres, R. B. LeFebvre, and J. M. Musser.** 2005. Genome sequence of a serotype M28 strain of group a streptococcus: potential new insights into puerperal sepsis and bacterial disease specificity. J. Infect. Dis. **192:**760–770.
11. **Hashikawa, S., Y. Iinuma, M. Furushita, T. Ohkura, T. Nada, K. Torii, T. Hasegawa, and M. Ohta.** 2004. Characterization of group C and G streptococcal strains that cause streptococcal toxic shock syndrome. J. Clin. Microbiol. **42:**186–192.
12. **Hirose, Y., K. Yagi, H. Honda, H. Shibuya, and E. Ozaki** 1997. Toxic shock-like syndrome caused by non-group A beta-hemolytic streptococci. Arch. Intern. Med. **157:**1891–1894.
13. **Igwe, E. I., P. L. Shewmaker, R. R. Facklam, M. M. Farley, C. van Beneden, and B. Beall.** 2003. Identification of superantigen genes speM, ssa, and smeZ in invasive strains of beta-hemolytic group C and G streptococci recovered from humans. FEMS Microbiol. Lett. **229:**259–264.
14. **Ikebe, T., A. Wada, Y. Inagaki, K. Sugama, R. Suzuki, D. Tanaka, A. Tamaru, Y. Fujinaga, Y. Abe, Y. Shimizu, H. Watanabe, and the Working Group for Group A Streptococci in Japan.** 2002. Dissemination of the phage-associated novel superantigen gene *speL* in recent invasive and noninvasive *Streptococcus pyogenes* M3/T3 isolates in Japan. Infect. Immun. **70:**3227–3233.
15. **Keiser, P., and W. Campbell.** 1992. 'Toxic strep syndrome' associated with group C Streptococcus. Arch. Intern. Med. **152:**882–884.
16. **Kline, J. B., and C. M. Collins.** 1996. Analysis of the superantigenic activity of mutant and allelic forms of streptococcal pyrogenic exotoxin A. Infect. Immun. **64:**861–869.
17. **Kotb, M., A. Norrby-Teglund, A. McGeer, H. El-Sherbini, M. T. Dorak, A. Khurshid, K. Green, J. Peeples, J. Wade, G. Thomson, B. Schwartz, and D. E. Low.** 2002. An immunogenetic and molecular basis for differences in outcomes of invasive group A streptococcal infections. Nat. Med. **8:**1398–1404.
18. **Kotzin, B. L., D. Y. Leung, J. Kappler, and P. Marrack.** 1993. Superantigens and their potential role in human disease. Adv. Immunol. **54:**99–166.
19. **Kugi, M., H. Tojo, I. Haraga, T. Takata, K. Handa, and K. Tanaka.** 1998. Toxic shock-like syndrome caused by group G Streptococcus. J. Infect. **37:** 308–309.
20. **Miyoshi-Akiyama, T., J. Zhao, H. Kato, K. Kikuchi, K. Totsuka, Y. Kataoka, M. Katsumi, and T. Uchiyama.** 2003. Streptococcus dysgalactiae-derived mitogen (SDM), a novel bacterial superantigen: characterization of its biological activity and predicted tertiary structure. Mol. Microbiol. **47:**1589–1599.
21. **Miyoshi-Akiyama, T., J. Zhao, K. Kikuchi, H. Kato, R. Suzuki, M. Endoh, and T. Uchiyama.** 2003. Quantitative and qualitative comparison of virulence traits, including murine lethality, among different M types of group A streptococci. J. Infect. Dis. **187:**1876–1887.
22. **Musser, J. M., V. Kapur, S. Kanjilal, U. Shah, D. M. Musher, N. L. Barg, K. H. Johnston, P. M. Schlievert, J. Henrichsen, D. Gerlach, et al.** 1993. Geographic and temporal distribution and molecular characterization of two highly pathogenic clones of Streptococcus pyogenes expressing allelic variants of pyrogenic exotoxin A (Scarlet fever toxin). J. Infect. Dis. **167:**337–346.
23. **Mwaka, M., T. Kato, R. Hayashi, T. Abe, T. Miyoshi-Akiyama, T. Uchiyama, and K. Imanishi.** 2003. Superantigenic stimulation of bovine T cells by Streptococcus dysgalactiae-derived mitogen (SDM). J. Tokyo Women's Med. Univ. **73:**24–34.
24. **Nakagawa, I., K. Kurokawa, A. Yamashita, M. Nakata, Y. Tomiyasu, N. Okahashi, S. Kawabata, K. Yamazaki, T. Shiba, T. Yasunaga, H. Hayashi, M. Hattori, and S. Hamada.** 2003. Genome sequence of an M3 strain of Streptococcus pyogenes reveals a large-scale genomic rearrangement in invasive strains and new insights into phage evolution. Genome Res. **13:**1042–1055.
25. **Natoli, S., C. Fimiani, N. Faglieri, L. Laurenzi, A. Calamaro, A. M. Frasca, and E. Arcuri.** 1996. Toxic shock syndrome due to group C streptococci. A case report. Intensive Care Med. **22:**985–989.
26. **Ojukwu, I. C., D. W. Newton, A. E. Luque, M. Y. Kotb, and M. Menegus.** 2001. Invasive group C Streptococcus infection associated with rhabdomyolysis and disseminated intravascular coagulation in a previously healthy adult. Scand. J. Infect. Dis. **33:**227–229.
27. **Page, R. D.** 1996. TreeView: an application to display phylogenetic trees on personal computers. Comput. Appl. Biosci. **12:**357–358.
28. **Proft, T., S. L. Moffatt, K. D. Weller, A. Paterson, D. Martin, and J. D. Fraser.** 2000. The streptococcal superantigen SMEZ exhibits wide allelic variation, mosaic structure, and significant antigenic variation. J. Exp. Med. **191:**1765–1776.
29. **Proft, T., P. D. Webb, V. Handley, and J. D. Fraser.** 2003. Two novel superantigens found in both group A and group C *Streptococcus*. Infect. Immun. **71:**1361–1369.
30. **Reda, K. B., V. Kapur, D. Goela, J. G. Lamphear, J. M. Musser, and R. R. Rich.** 1996. Phylogenetic distribution of streptococcal superantigen SSA allelic variants provides evidence for horizontal transfer of *ssa* within *Streptococcus pyogenes*. Infect. Immun. **64:**1161–1165.
31. **Sachse, S., P. Seidel, D. Gerlach, E. Gunther, J. Rodel, E. Straube, and K. H.**

Schmidt. 2002. Superantigen-like gene(s) in human pathogenic Streptococcus dysgalactiae, subsp equisimilis: genomic localisation of the gene encoding streptococcal pyrogenic exotoxin G (speG(dys)). FEMS Immunol. Med. Microbiol. **34:**159–167.
32. **Sali, A., and T. L. Blundell.** 1993. Comparative protein modelling by satisfaction of spatial restraints. J. Mol. Biol. **234:**779–815.
33. **Smoot, J. C., K. D. Barbian, J. J. Van Gompel, L. M. Smoot, M. S. Chaussee, G. L. Sylva, D. E. Sturdevant, S. M. Ricklefs, S. F. Porcella, L. D. Parkins, S. B. Beres, D. S. Campbell, T. M. Smith, Q. Zhang, V. Kapur, J. A. Daly, L. G. Veasy, and J. M. Musser.** 2002. Genome sequence and comparative microarray analysis of serotype M18 group A Streptococcus strains associated with acute rheumatic fever outbreaks. Proc. Natl. Acad. Sci. USA **99:**4668–4673.
34. **Sumby, P., S. F. Porcella, A. G. Madrigal, K. D. Barbian, K. Virtaneva, S. M. Ricklefs, D. E. Sturdevant, M. R. Graham, J. Vuopio-Varkila, N. P. Hoe, and J. M. Musser.** 2005. Evolutionary origin and emergence of a highly successful clone of serotype M1 group a Streptococcus involved multiple horizontal gene transfer events. J. Infect. Dis. **192:**771–782.
35. **Thompson, J. D., D. G. Higgins, and T. J. Gibson.** 1994. CLUSTAL W: improving the sensitivity of progressive multiple sequence alignment through sequence weighting, position-specific gap penalties and weight matrix choice. Nucleic Acids Res. **22:**4673–4680.
36. **Uchiyama, T., Y. Kamagata, X. J. Yan, M. Kohno, M. Yoshioka, H. Fujikawa, H. Igarashi, M. Okubo, F. Awano, T. Saito-Taki, et al.** 1987. Study of the biological activities of toxic shock syndrome toxin-1. II. Induction of the proliferative response and the interleukin 2 production by T cells from human peripheral blood mononuclear cells stimulated with the toxin. Clin. Exp. Immunol. **68:**638–647.
37. **Uchiyama, T., X. J. Yan, K. Imanishi, and J. Yagi.** 1994. Bacterial superantigens—mechanism of T cell activation by the superantigens and their role in the pathogenesis of infectious diseases. Microbiol. Immunol. **38:**245–256.
38. **Wagner, J. G., P. M. Schlievert, A. P. Assimacopoulos, J. A. Stoehr, P. J. Carson, and K. Komadina.** 1996. Acute group G streptococcal myositis associated with streptococcal toxic shock syndrome: case report and review. Clin. Infect. Dis. **23:**1159–1161.

Editor: A. Camilli

RESEARCH LETTER

Positive correlation between low adhesion of group A *Streptococcus* to mammalian cells and virulence in a mouse model

Tohru Miyoshi-Akiyama[1], Jizi Zhao[1,2], Takehiko Uchiyama[3], Junji Yagi[3] & Teruo Kirikae[1]

[1]Department of Infectious Diseases, International Medical Center of Japan, Research Institute, Toyama, Shinjuku-ku, Tokyo, Japan; [2]Department of Special Pathogen, International Research Center for Infectious Disease, Research Institute for Microbial Disease, Osaka University, Yamadaoka, Suita, Osaka, Japan; and [3]Department of Microbiology and Immunology, Tokyo Women's Medical University, Kawada-cho, Shinjuku-ku, Tokyo, Japan

Correspondence: Tohru Miyoshi-Akiyama, Department of Infectious Diseases, International Medical Center of Japan, Research Institute, 1-21-1, Toyama, Shinjuku-ku, Tokyo, 162-8655, Japan. Tel.: +81 3 3202 7181, ext. 2903; fax: +81 3 3202 7364; e-mail: takiyam@ri.imcj.go.jp

Received 10 October 2008; accepted 11 January 2009.
First published online 12 February 2009.

DOI:10.1111/j.1574-6968.2009.01513.x

Editor: Jan-Ingmar Flock

Keywords
Streptococcus; STSS; GAS; adhesin; *in vivo* model.

Abstract

We previously reported that a mouse model reflected, at least in part, the pathogenic mechanism of bacteremia observed during streptococcal toxic shock syndrome caused by group A *Streptococcus* (GAS). We have extended this study by assaying the *in vitro* adhesion of these same isolates to mammalian cells. Unexpectedly, we found that high-virulence GAS isolates in the mouse model showed low adhesion to the host cells. Similarly, the rate of recovery from the peritoneal cavity and cardiac blood of mice after intraperitonial injection was higher for high- than for low-virulence strains. Levels of expression of molecules that affect the adhesion of GAS to host cells were not significantly correlated with GAS virulence. Taken together, these results indicate that the invasiveness of GAS, reflected as higher virulence, is correlated directly with lower adhesion to host cells.

Introduction

The group A streptococci (GAS) cause various infectious disease, including invasive streptococcal toxic shock syndrome (STSS), which can be lethal (Smith *et al.*, 2005). Epidemiological studies have shown that GAS strains carrying *emm1* and *emm3* are more frequently isolated from STSS than strains carrying *emm4*, and *emm12*. Because GAS usually do not show significant virulence in mice, there has been no good mouse model reflecting the pathogenic mechanism of STSS. To analyze the pathogenic mechanism of GAS, we compared the virulence in mice of GAS clinical isolates carrying *emm1*, *emm3*, *emm4* and *emm12* by injecting these isolates into mouse peritoneal cavities. We found that GAS isolates carrying *emm1* and *emm3* showed higher virulence than those carrying *emm4* and *emm12*, indicating that this mouse model reflected, at least in part, the pathogenic mechanism of bacteremia observed during STSS (Shiseki *et al.*, 1999; Miyoshi-Akiyama *et al.*, 2003).

Adhesion of bacteria to the host cell is considered one of the most important processes in bacterial infection (Kerr, 1999; Raupach *et al.*, 1999). Many GAS products are known as adherence factors (Molinari *et al.*, 1997; Schrager & Wessels, 1997; Fluckiger *et al.*, 1998; Jadoun *et al.*, 1998; Terao *et al.*, 2001, 2002a; Mora *et al.*, 2005). Testing of the relationship between GAS adherence and virulence in animal models (Courtney *et al.*, 1994; Wessels & Bronze, 1994; Terao *et al.*, 2001, 2002b) has shown that, like other bacteria, GAS requires an adhesion step to colonize the host. In contrast to other types of GAS infection, GAS spreads rapidly throughout the body in individuals with STSS, making it likely that GAS causing STSS has particular features that allow it to interact with and adhere to the host cell.

While assessing our mouse model of STSS, we constructed a panel of GAS isolates with known virulence against mice following intraperitonial infection. In this study, we examined the adherence of these GAS isolates to mammalian cells. Unexpectedly, we found that isolates with higher virulence in mice showed lower adherence to mammalian cells. Our findings suggest that the adhesion of GAS to mammalian cells reduces virulence in our mouse model.

Materials and methods

Bacterial isolates and media

Profiles of GAS clinical isolates used in this study are summarized in Table 1. To prevent phenotypic changes of the isolates during passage, all isolates were stored at −80 °C until use. The GAS isolates were cultured in Brain–Heart Infusion broth (Difco) overnight in the presence of 5% CO_2 at 37 °C. The lethal dose 50% (LD_{50}) values indicated in Table 1 were based on our previous study (Shiseki *et al.*, 1999). In that study, GAS suspended at 0.5 mL of phosphate buffered saline (PBS) and fivefold serial dilutions was injected intraperitonially into female 6-week-old *ddY* mice (SLC Japan; 10 mice per group). The mice were observed for 3 days and the LD_{50} was calculated.

emm typing and pulsed-field gel electrophoresis (PFGE)

emm typing of the GAS isolates was performed as described (http://www.cdc.gov/ncidod/biotech/strep/strepindex.htm) with minor modifications. GAS isolates were compared by PFGE using a GenePath system (Bio-Rad) with SmaI digestion, as described (Miyoshi-Akiyama *et al.*, 2003).

GAS adhesion to mammalian cells

The mammalian cell lines used in this study included the mouse fibroblast cell line, L cells, as well as HeLa and HEp-2 cells. These cells were precultured overnight in 2 mL of Roswell Park Memorial Institute medium (RPMI) 1640 containing 10% fetal calf serum (FCS) at 1×10^5 cell per well in 24-well culture plates. One hour before using the cells, the medium was replaced with 1 mL of fresh RPMI 1640 containing 10% FCS. The concentrations of overnight cultures of GAS isolates were adjusted to an $OD_{600\,nm}$ of 0.02, and a 20-μL aliquot of each GAS suspension, containing *c.* 2×10^4 CFU of bacteria, was added to the mammalian cell cultures (MOI = 0.2). After 4 h of incubation in a humidified 5% CO_2 incubator at 37 °C, each well was washed five times with 1 mL of PBS, and 500 μL of DDW was added to disrupt the cells. After vortexing for 30 s, the suspensions were plated on duplicate sheep blood agar plates to determine the number of CFU. To analyze bacterial growth, the bacteria were recovered by centrifugation and the number was counted by plating as described above. To microscopically assay the adherence of GAS to L cells, the cells were cultured in chamber slides (Lab-Tek) with the GAS isolates, washed using the same conditions as described above, and the cells were subjected to conventional Giemsa staining.

Recovery of GAS from the abdominal cavity and bloodstream after intraperitonial injection

The $OD_{600\,nm}$ values of GAS isolates were adjusted to 2 and 20 with PBS for recovery from the peritoneal cavity and bloodstream, respectively, and 0.5 mL of each suspension was injected intraperitonial into *ddY* mice (four animals per GAS isolate). Under these conditions, *c.* 1×10^8 and

Table 1. Profiles of the GAS isolates in this study

Disease	Isolate name	Sites of isolation in mice	Fate of the patients	*emm* type	LD_{50} (CFU per mouse)*
STSS	ST1	Blood, pharynx	Recovered	*emm3*	8.33×10^3
	ST2	Blood, necrotic tissues	Died	*emm89*	2.51×10^5
	ST3	Blood, necrotic tissues	Died	*emm3*	1.12×10^6
	ST4	Blood, necrotic tissues	Died	*emm3*	2.51×10^6
	ST5	Pharynx	Recovered	*emm3*	9.97×10^6
	ST6	Blood	Died	*emm3*	1.68×10^6
	ST7	Blood	Died	*emm3*	6.31×10^7
	ST8	Blood	Recovered	*emm4*	7.94×10^7
	ST9	Blood, necrotic tissues	Died	*emm22.2*	2.51×10^8
	ST10	Blood, necrotic tissues	Died	*emm4*	5.53×10^7
Scarlet fever	SF1	Pharynx	Recovered	*emm1*	9.13×10^6
	SF2	Pharynx	Recovered	*emm13w*	2.51×10^8
	SF3	Pharynx	Recovered	*emm11*	2.82×10^8
	SF4	Pharynx	Recovered	*emm4*	3.55×10^8
	SF5	Pharynx	Recovered	*emm4*	3.98×10^8
	SF6	Pharynx	Recovered	*emm12*	4.47×10^8
	SF7	Pharynx	Recovered	*emm4*	5.01×10^8
	SF8	Pharynx	Recovered	*emm12*	1.80×10^7
	SF9	Pharynx	Recovered	*emm12*	1.25×10^7
	SF10	Pharynx	Recovered	*emm4*	3.36×10^7

*Based on Shiseki *et al.* (1999).

1×10^9 CFU per mouse were injected for recovery from the peritoneal cavity and bloodstream, respectively. The actual number of bacterial cells inoculated was confirmed by plating, as described above, and there was no significant difference among the isolates (data not shown). To recover bacterial cells from the peritoneal cavity, the latter was rinsed with 3 mL PBS 30 min after injection, and the collected PBS was used as the sample. To recover bacteria from the bloodstream, blood samples were obtained by cardiac puncture 3 h after injection. These samples were plated on sheep blood agar plates as described above.

Immunoblotting against M proteins

The constant region of the M6 protein gene was amplified by standard PCR using primers containing a BamHI site (5′-GGGAGGGGATCCGCATCACGTGAAGCTTAAGAAA-3′) and a SalI site (5′-AGTGGCGTCGACTTAGTTTTCTTCTTTGGGTTT-3′), and cloned into the corresponding sites of the his-tag expression vector, pQE30 (Qiagen). The resulting plasmid was introduced into *Escherichia coli* XL1-blue (Stratagene) and recombinant protein of the constant region of M6 was expressed using isopropyl-β-D-thiogalactopyranoside, and purified by affinity to Ni-chelate resin, as described by the manufacturers. The protein was further purified by cation-exchange column chromatography, and injected into rabbits using standard procedures. These antisera were used for immunoblotting. GAS isolates were cultured as above. After adjusting the bacterial cell number by measuring the OD, the cells were lysed in sodium dodecyl sulfate-polyacrylamide gel electrophoresis (SDS-PAGE) sample buffer and subjected to standard SDS-PAGE followed by electroblotting on polyvinylidene difluoride (PVDF) membranes (NEN Life Science Products). Proteins were visualized using ECL (GE healthcare).

Hyaluronic acid quantification

Quantification of the amount of hyaluronic acid in each GAS isolate, using Stains-All (Sigma-Aldrich), was performed as described (Miyoshi-Akiyama *et al*., 2003).

Far-Western blotting using fibronectin as a probe

To compare the profile of fibronectin-interacting proteins produced by each GAS isolate, far-Western blotting was performed using fibronectin as a probe. PVDF filters blotted with GAS lysates were prepared as described above. The filters were incubated with 10 μg mL^{-1} of fibronectin (Upstate Biotechnology), and the binding of fibronectin to the GAS proteins was detected using rabbit antifibronectin polyclonal antibody (Biomedicals Inc.) with the chemiluminescence systems described above.

Statistical analysis

Data were analyzed for significance by the Kendall's rank correlation test for nonparametric data. These analyses were performed using STAT-MACROS for MS-EXCEL (http://www.tuat.ac.jp/~ethology/Columbo/Stat/index.html), and $P < 0.05$ was used to indicate statistical significance.

Results

PFGE pattern and *emm* type of the GAS isolates

When we analyzed the GAS isolates used in this study by PFGE after SmaI digestion, we found that their PFGE patterns agreed with those reported previously (Stanley *et al*., 1995; Murase *et al*., 1999) (Fig. 1). ST1 to ST7 showed the same PFGE pattern without any polymorphism, although the *emm* type of ST2, *emm89*, differs from the type, *emm3*, in ST1 and ST3 to ST7. Thus, ST1 to ST7 have similar genetic backgrounds. The other isolates with *emm4* (ST8, ST10, SF4, SF5, SF7, and SF10) or *emm12* (SF6, SF8, and SF9) showed PFGE patterns that differed from each other.

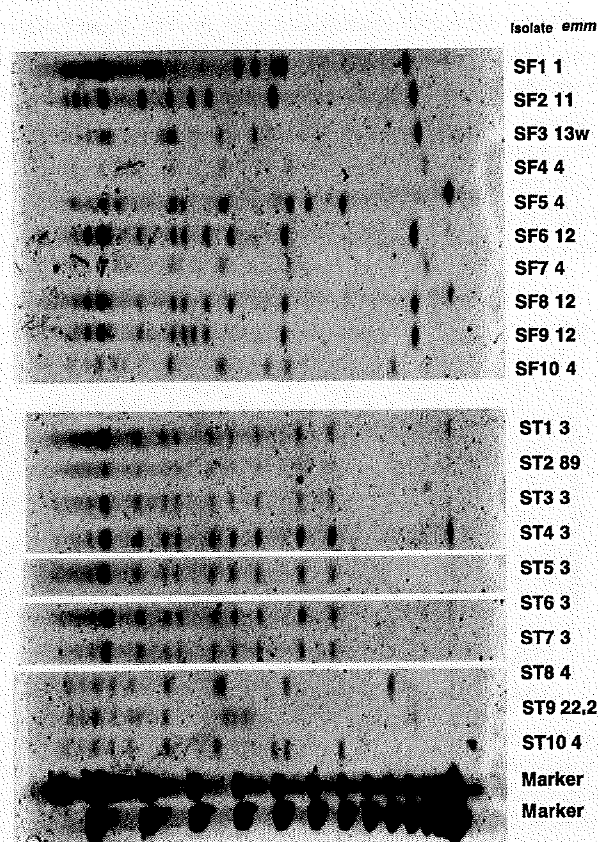

Fig. 1. PFGE patterns of the GAS isolates used in this study. The GAS isolates were digested with SmaI and analyzed by PFGE. The names of the isolates and their *emm* types are shown.

Adherence of GAS isolates to mammalian cells

To compare the ability of these GAS isolates to adhere to mammalian cells, we utilized L cells, a mouse fibroblast cell line. The adhesion of these GAS isolates to L cells showed a significant inverse association with their virulence in mice ($P = 0.0025$) (Fig. 2a). During the period of coculture with L cells (4 h), all isolates except ST10 showed essentially the same growth behavior (data not shown). When L cells were treated with the least virulent isolate, SF10, but not the most virulent isolate, ST1, GAS bacterial cells were observed on the surface of L cells. However, there was no difference in appearance between L cells incubated with SF10 and ST1, indicating that the difference in adhesion ability between these two isolates was not due to physical modification of L cells, such as disappearance from the assay system (Fig. 2b). The lower adherence of ST1 compared with SF10 was also observed when these isolates were incubated with the human-derived cell lines HEp-2 and HeLa (Fig. 2c), although the difference in adhesion between ST1 and SF10 was relatively small. These results indicated that high-virulence GAS isolates have lower ability to adhere to mammalian cells than low-virulence isolates.

To confirm that high-virulence GAS isolates have lower ability to adhere to mammalian cells *in vivo*, these isolates were injected into mice (intraperitonially) and recovered from the peritoneal cavity 30 min later. When we plotted the number of bacteria recovered for each isolate against its corresponding virulence, we found that GAS virulence in mice was correlated positively with GAS recovery from the peritoneal cavity ($P < 0.00001$; Fig. 3). As recovery was performed 30 min after injection, it is highly unlikely that the observed differences in number of bacteria recovered were due to bacterial growth. We previously reported that phagocytic cells (neutrophils) were induced by intraperitonial administration of GAS in mice (Miyoshi-Akiyama *et al.*, 2005). This induction required at least 3 h and maximized 12 h after GAS inoculation. Thus, the contribution of phagocytic killing of bacterial cells to the number of GAS recovered from peritoneal cavity was also minimal. These

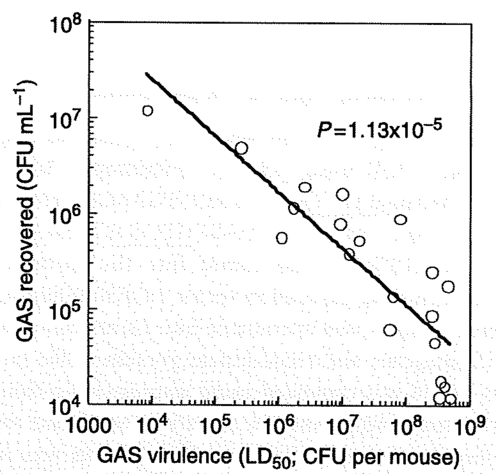

Fig. 3. Correlation of virulence with GAS recovery from the peritoneal cavity after intraperitonial injection into mice. GAS were recovered from the peritoneal cavities of mice 30 min after intraperitonial injection of the GAS isolates suspended in PBS, as described in Materials and methods. The number of GAS recovered (CFU mL^{-1}) was plotted against virulence in mice (LD$_{50}$; CFU per mouse). The correlation was analyzed by Kendall's rank correlation analysis ($P = 1.13 \times 10^{-5}$).

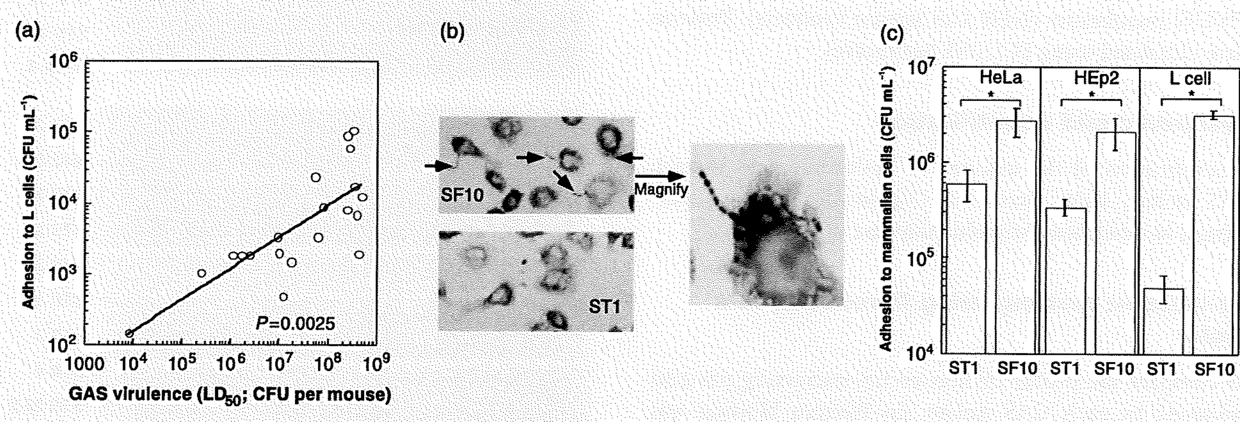

Fig. 2. Adhesion of the GAS isolates to mammalian cells. (a) Correlation of the lower adhesion of the isolates with virulence in the mouse model. Adhesion of the GAS isolates to L cells was analyzed as described in Materials and methods, and the numbers of adhering GAS cells (CFU mL^{-1}) were plotted against the mouse virulence (LD$_{50}$; CFU per mouse). During the 4-h analysis period, all isolates except ST10 showed essentially the same growth behavior (data not shown). Correlations were analyzed by Kendall's rank correlation analysis ($P = 0.0025$). (b) L cells were incubated with SF10 (the least virulent isolate) or ST1 (the most virulent isolate) as described in Materials and methods. After washing with PBS, Giemsa staining was performed. Bacterial cells seen in L cells are marked with arrows in the figure. (c) The indicated cell lines were incubated with SF10 or ST1 to compare differences in GAS adhesion. The data are presented as means ± SE. Statistical significance of the difference of ability to adhere cell lines between ST1 and SF10 were analyzed by Student's *t*-test ($^{*}P < 0.01$).

results indicated that GAS isolates that showed higher recovery rates were trapped less frequently in the mouse peritoneal cavity than GAS isolates that showed lower recoveries.

GAS invasion into the bloodstream in mice

Next we investigated whether there was a correlation between the invasiveness of GAS isolates into the bloodstream and lethality in mice. The GAS isolates were injected into mice (intraperitonially), and blood samples were obtained by cardiac puncture 3 h later. We found that the appearance of GAS in the bloodstream after injection into the peritoneal cavity was significantly correlated with virulence ($P < 0.00001$, Fig. 4), suggesting that GAS isolates not trapped on host cells due to their lower ability to attach appear in the bloodstream more rapidly than GAS isolates that attach more efficiently to the host cells. Our results agree with previous findings, showing that GAS isolated from the blood shows lower adherence than GAS isolated from the throat or skin (Molinari & Chhatwal, 1998).

Comparison of molecular features of the GAS isolates

As the low adhesion of GAS to L cells was correlated with high virulence in mice, the lower adherence reflects the ability of GAS to spread in the body. To identify possible candidates that may affect the ability to adhere to host cells, we examined the expression patterns of molecules reported as 'adhesins' of GAS.

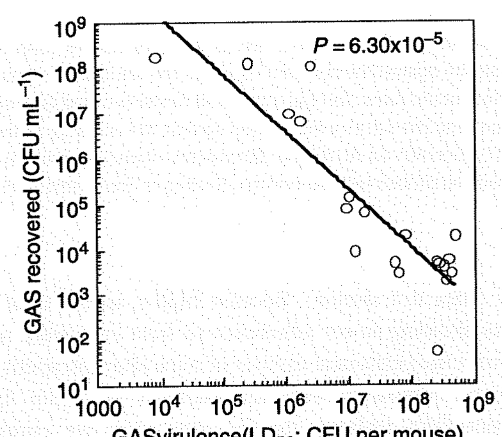

Fig. 4. Correlation of virulence with GAS recovery in heart blood after intraperitonial injection into mice. GAS were recovered by puncture of the heart 3 h after intraperitonial injection of the GAS isolates suspended in PBS as described in Materials and methods. The number of GAS recovered (CFU mL^{-1}) was plotted against virulence in mice (LD_{50}; CFU per mouse). The correlation was analyzed by Kendall's rank correlation analysis ($P = 6.30 \times 10^{-5}$).

GAS with mutations in the M protein and protein F genes showed markedly decreased host cell adhesion (Okada *et al.*, 1994). To compare the expression level of M protein among the GAS isolates, an antibody against the constant region of M6 protein was used for Western blotting analysis (Fig. 5a). It is not appropriate to compare the M protein expression levels among GAS isolates carrying different types of *emm*, such as *emm4*, *emm3*, and *emm12*. ST1 to ST7, however, have similar genetic backgrounds, as shown on PFGE analysis (Fig. 1), although these isolates showed marked differences in adhesion to L cells and virulence in mice. There were no significant differences in M protein expression level among these seven isolates, suggesting that M protein is not responsible for the difference in the ability of GAS isolates to adhere to host cells.

Because the hyaluronic capsule content of GAS isolates has been reported to act as an adherence factor via binding with CD44 (Schrager *et al.*, 1998; Darmstadt *et al.*, 2000), to prevent phagocytic killing in co-operation with M protein, we assessed the hyaluronic acid capsule content in each GAS isolate. There was no correlation between the hyaluronic acid content of each GAS isolate and its virulence (Fig. 5b) ($P > 0.9$). Although ST1, which has a mucoid phenotype, showed the highest hyaluronic acid content, other isolates showed similar hyaluronic acid levels. These observations suggest that differences in hyaluronic acid content among the isolates cannot explain the observed differences in their virulence.

We also examined the profile of fibronectin-binding proteins produced by the GAS isolates. GAS produces many factors that bind fibronectin (Bisno *et al.*, 2003), one of the major extracellular matrix proteins. Because distribution of the fibronectin-binding proteins in GAS depends to some extent on their *emm* type (Kratovac *et al.*, 2007) and the *emm* types of the isolates used in this study differ from each other, we performed far Western blotting, using fibronectin as a probe, to distinguish among them (Fig. 5c). Several proteins were detected in each isolate, and there were similarities among the profiles of the different isolates. By PCR, we confirmed that M1 and M3 type GAS, corresponding to the ST1, ST3-7, and SF1 isolates, do not carry the protein F gene (data not shown). Probing with fibronectin, however, detected proteins of around 110–130 kDa in ST3 to ST6 and 70–100 kDa in ST1 and ST2. Although proteins from the GAS isolates carrying *emm* other than *emm3* (and *emm89*) showed reactivity with fibronectin, their expression level was not correlated with virulence or adhesion, suggesting that fibronectin-reactive proteins of GAS are not responsible for the differences in their ability to adhere to host cells.

Discussion

Our results are somewhat surprising, as GAS virulence was negatively correlated with the ability to adhere to

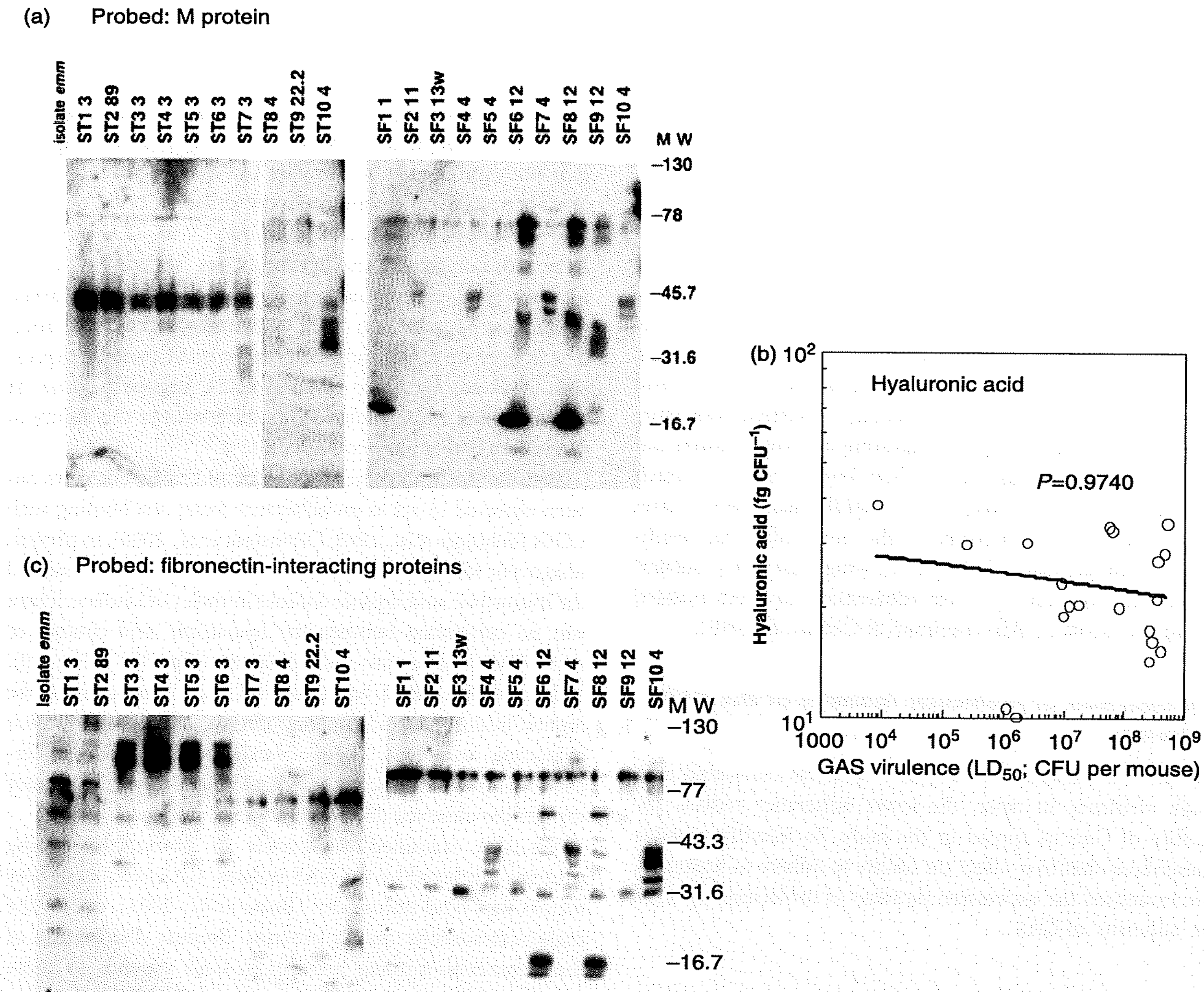

Fig. 5. Analyses of traits related to mammalian cell adhesion of the GAS isolates. (a) M protein expression level in the GAS isolates. GAS lysates, prepared as described in Materials and methods, were blotted and probed with antiserum against the constant region of the M6 protein. Because of differences in M-types among the isolates, the molecular weights of the M proteins are not the same. (b) Hyaluronic acid contents of the GAS isolates. Hyaluronic acid was quantified using Stains-All as described in Materials and methods, and the values were plotted against the virulence of the GAS isolates in mice. The correlation was analyzed by Kendall's rank correlation analysis ($P=0.9740$). (c) Analysis of fibronectin-interacting proteins in the GAS isolates. GAS lysates prepared as described in Materials and methods were blotted and probed with fibronectin. Binding of fibronectin to the GAS proteins was detected with antifibronectin antibody.

mammalian cells. Assessments of the adhesion of GAS isolates from STSS and other GAS infectious diseases, such as superficial disease, showed only slight differences between them (Bennett-Wood *et al.*, 1998). In the present study, however, we found 10–100-fold differences between isolates using L cells as mammalian host cells. Among the mammalian cells tested, L cells showed the highest differences in the adherence ability of GAS isolates, suggesting that the discrepancies between our results and those of previous studies may be due to differences in the cell lines used. The inverse correlation between adherence to L cells and virulence in mice was maintained in additional 32 GAS clinical isolates tested (data not shown). Because higher amounts of GAS isolates showing lower adherence to host cells were recovered from the peritoneal cavities of mice after intraperitonial injection, compared with the recovery of more highly adherent GAS isolates, the *in vitro* assay we employed reflected *in vivo* conditions, at least in this mouse model.

Several previous studies have shown that the genetic disruption of GAS molecules that affect bacterial adherence to mammalian cells attenuated the virulence in mouse models (Terao *et al.*, 2001, 2002b; Okamoto *et al.*, 2004). These findings, however, differed from our results and from those of a previous study regarding protein F1 (Nyberg *et al.*, 2004). This discrepancy may be due, at least in part, to the route of GAS injection; some of the former studies employed subcutaneous and intranasal injections, while the latter studies and ours employed the intraperitonial route. Intraperitoneal injection makes it possible for GAS to gain direct access to normally sterile sites within the body without a previous colonization step. In many patients with STSS, GAS enters through an injury or wound. In such cases, GAS isolates that do not adhere tightly to the host cells could spread more rapidly in the body than those that become trapped at sites by adhesion to host cells. Intraperitoneal injection of GAS may mimic this process. Adhesion is clearly necessary for other types of GAS infectious diseases, such as pharyngitis. In these individuals, GAS attaches to host cells at other locations, such as the throat, and may then colonize the site to begin the infection. The transcriptome of GAS has been reported to change dramatically, allowing GAS to spread after entry into the sterile part of the body (Graham *et al.*, 2006). Our findings, based on these phenotypic analyses, support these previous findings

Acknowledgements

The authors thank Dr K. Ooe and Dr Y. Shimizu of Asahi General Hospital, and Dr T. Kikuchi of Kikuchi Clinic for providing the GAS isolates. We also thank Dr K. Kikuchi of Tokyo Women's Medical University for technical assistance regarding PFGE analysis. T.M.-A. was supported by grants-in-aid from the Ministry of Education, Culture, Sports, Science, and Technology of Japan.

References

Bennett-Wood VR, Carapetis JR & Robins-Browne RM (1998) Ability of clinical isolates of group A streptococci to adhere to and invade HEp-2 epithelial cells. *J Med Microbiol* **47**: 899–906.

Bisno AL, Brito MO & Collins CM (2003) Molecular basis of group A streptococcal virulence. *Lancet Infect Dis* **3**: 191–200.

Courtney HS, Bronze MS, Dale JB & Hasty Dl (1994) Analysis of the role of M24 protein in group A streptococcal adhesion and colonization by use of omega-interposon mutagenesis. *Infect Immun* **62**: 4868–4873.

Darmstadt GL, Mentele L, Podbielski A & Rubens CE (2000) Role of group A streptococcal virulence factors in adherence to keratinocytes. *Infect Immun* **68**: 1215–1221.

Fluckiger U, Jones KF & Fischetti VA (1998) Immunoglobulins to group A streptococcal surface molecules decrease adherence to and invasion of human pharyngeal cells. *Infect Immun* **66**: 974–979.

Graham MR, Virtaneva K, Porcella SF *et al.* (2006) Analysis of the transcriptome of group A *Streptococcus* in mouse soft tissue infection. *Am J Pathol* **169**: 927–942.

Jadoun J, Ozeri V, Burstein E, Skutelsky E, Hanski E & Sela S (1998) Protein F1 is required for efficient entry of *Streptococcus pyogenes* into epithelial cells. *J Infect Dis* **178**: 147–158.

Kerr JR (1999) Cell adhesion molecules in the pathogenesis of and host defence against microbial infection. *Mol Pathol* **52**: 220–230.

Kratovac Z, Manoharan A, Luo F, Lizano S & Bessen DE (2007) Population genetics and linkage analysis of loci within the FCT region of *Streptococcus pyogenes*. *J Bacteriol* **189**: 1299–1310.

Miyoshi-Akiyama T, Zhao J, Kikuchi K, Kato H, Suzuki R, Endoh M & Uchiyama T (2003) Quantitative and qualitative comparison of virulence traits, including murine lethality, among different M types of group A streptococci. *J Infect Dis* **187**: 1876–1887.

Miyoshi-Akiyama T, Takamatsu D, Koyanagi M, Zhao J, Imanishi K & Uchiyama T (2005) Cytocidal effect of *Streptococcus pyogenes* on mouse neutrophils *in vivo* and the critical role of streptolysin S. *J Infect Dis* **192**: 107–116.

Molinari G & Chhatwal GS (1998) Invasion and survival of *Streptococcus pyogenes* in eukaryotic cells correlates with the source of the clinical isolates. *J Infect Dis* **177**: 1600–1607.

Molinari G, Talay SR, Valentin-Weigand P, Rohde M & Chhatwal GS (1997) The fibronectin-binding protein of *Streptococcus pyogenes*, SfbI, is involved in the internalization of group A streptococci by epithelial cells. *Infect Immun* **65**: 1357–1363.

Mora M, Bensi G, Capo S, Falugi F, Zingaretti C, Manetti AG, Maggi T, Taddei AR, Grandi G & Telford JL (2005) Group A *Streptococcus* produce pilus-like structures containing protective antigens and Lancefield T antigens. *P Natl Acad Sci USA* **102**: 15641–15646.

Murase T, Suzuki R, Osawa R & Yamai S (1999) Characteristics of *Streptococcus pyogenes* serotype M1 and M3 isolates from patients in Japan from 1981 to 1997. *J Clin Microbiol* **37**: 4131–4134.

Nyberg P, Sakai T, Cho KH, Caparon MG, Fassler R & Bjorck L (2004) Interactions with fibronectin attenuate the virulence of *Streptococcus pyogenes*. *EMBO J* **23**: 2166–2174.

Okada N, Pentland AP, Falk P & Caparon MG (1994) M protein and protein F act as important determinants of cell-specific tropism of *Streptococcus pyogenes* in skin tissue. *J Clin Invest* **94**: 965–977.

Okamoto S, Kawabata S, Terao Y, Fujitaka H, Okuno Y & Hamada S (2004) The *Streptococcus pyogenes* capsule is required for adhesion of bacteria to virus-infected alveolar epithelial cells and lethal bacterial–viral superinfection. *Infect Immun* **72**: 6068–6075.

Raupach B, Mecsas J, Heczko U, Falkow S & Finlay BB (1999) Bacterial epithelial cell cross talk. *Curr Top Microbiol* **236**: 137–161.

Schrager HM & Wessels MR (1997) Hyaluronic acid capsule modulates interactions of group A streptococci with human epidermal keratinocytes. *Adv Exp Med Biol* **418**: 517–523.

Schrager HM, Alberti S, Cywes C, Dougherty GJ & Wessels MR (1998) Hyaluronic acid capsule modulates M protein-mediated adherence and acts as a ligand for attachment of